P-05-66

Forsmark site investigation

Evaluation of the overcoring results from borehole KFM01B

Ulf Lindfors, Fredrik Perman, Jonny Sjöberg
SwedPower AB

April 2005

Svensk Kärnbränslehantering AB
Swedish Nuclear Fuel
and Waste Management Co
Box 5864
SE-102 40 Stockholm Sweden
Tel 08-459 84 00
+46 8 459 84 00
Fax 08-661 57 19
+46 8 661 57 19

ISSN 1651-4416
SKB P-05-66

Forsmark site investigation

Evaluation of the overcoring results from borehole KFM01B

Ulf Lindfors, Fredrik Perman, Jonny Sjöberg
SwedPower AB

April 2005

Keywords: AP PF 400-04-16, Stress state, Confidence intervals, Geological correlation, Core damage.

Summary

The work reported here comprised an evaluation and interpretation of the overcoring stress measurement data from borehole KFM01B in a broader, geological-rock mechanics perspective. The work included (i) comparison and correlation of geological data with measurement results, (ii) examination of core discing observations, (iii) examination of thin sections from a selected overcore sample to determine the extent of microcracking, and (iv) estimation of stress state from core discing and/or microcracking.

The results showed that measurements at Level 1 were located in much better rock in terms of fracture frequency than at Level 2. The presence of fractures on Level 2 probably led to lower local stresses, which permitted measurements to be taken, whereas the overall stress state at larger depth is likely to have been higher. No clear correlations could be found between rock types and measurement results, and the difference in stress orientation measured at Level 1 and Level 2 could not be correlated to the presence of e.g. geological structures.

Data on core discing indicated a maximum horizontal stress of around 35 MPa for Level 1, which is in very close agreement with the stress state obtained from the overcoring measurements. For Level 2, core discing information indicated stresses of at least 40–48 MPa magnitude (for a disc thickness of 12 mm). The observations of thinner discs at the locations of the successful measurements, as well as the observations of discing of solid core, point towards local stress magnitudes in excess of 40–48 MPa.

Examination of thin sections revealed signs of initiating spalling failure at the pilot hole wall. Spalling failure can, in turn, be a possible explanation to the observed premature debonding of strain gauges for several overcoring tests on Level 2. Stress estimations based on the assumption of developed spalling failures indicated a maximum horizontal stress between 43 and 53 MPa for Level 2. P-wave velocity measurements partly supported the observed core damage (at large depths), but could not be used to determine stress orientations.

In conclusion, the presented stress estimates from using indirect methods confirm, to a large extent, the stress state inferred from overcoring data alone. The maximum horizontal stress in borehole KFM01B reaches 35 MPa already at approximately 250 m depth. Higher stresses are likely at larger depths – the indirect evidence from this study suggests that stresses at 400 to 450 m depths reach at least 40 MPa. Core discing data from Level 2 indicate that the maximum horizontal stress may be higher at these depths.

Sammanfattning

Denna rapport presenterar en utvärdering och tolkning av bergspänningsmätningar med överborrningsmetoden utförda i borrhål KFM01B, utifrån ett vidare, geologiskt-bergmekaniskt perspektiv. Arbetet innefattade: (i) jämförelse och korrelation av geologiska data med mätresultat, (ii) undersökning av ”core discing” (uppsprickning av borrkärnor i ringformade bitar), (iii) undersökning av tunnslip från en utvald överborrningskärna i syfte att bestämma omfattning av mikrouppsprickning samt (iv) uppskattning av spänningarna från ”core discing” och/eller mikrouppsprickning.

Resultaten visade att mätningar på mätnivå 1 var utförda i berg av bättre kvalitet med avseende på sprickfrekvens, jämfört med mätningar på nivå 2. Närvaron av sprickor på mätnivå 2 resulterade troligen i lägre spänningar lokalt, vilket i sin tur medgav att mätningar kunde utföras (utan besvärande ”core discing”). Det är dock troligt att det generellt sett rådande spänningsfältet är högre på dessa större djup. Det fanns ingen tydlig korrelation mellan bergarter och mätresultat. Skillnaden i uppmätt spänningsriktning mellan nivå 1 och 2 kunde inte heller korreleras till exempelvis geologiska strukturer i borrhålet.

Data från ”core discing” indikerade en maximal horisontell spänning på ca 35 MPa på mätnivå 1. Detta är i mycket nära överensstämmelse med spänningsdata från överborrningsmätningar. ”Core discing” på mätnivå 2 indikerade en horisontalspänning på minst 40–48 MPa (för 12 mm ringtjocklek). Observationer av tunnare ringar i lägen för där överborrningsmätningar utförts, samt observationer av ”core discing” på solid kärna, tyder på att spänningsmagnituden lokalt kan överskrida 40–48 MPa.

Undersökning av tunnslip visade tecken på begynnande spjälkning i pilothålsväggen. Spjälkbrott kan, i sin tur, vara en bidragande orsak till att töjningsgivare släppt från pilothålsväggen i ett tidigt skede av överborrningsprocessen, vilket observerats i flera fall på mätnivå 2. Bakåträknade spänningar för spjälkbrott uppgick till mellan 43 och 53 MPa för mätnivå 2. Mätningar av p-vågshastigheten bekräftade delvis uppkomna skador i borrkärnor (på stort djup), men kunde inte nyttjas för bestämning av spänningsriktningar.

Sammanfattningsvis bekräftar spänningsuppskattningarna med de indirekta metoderna de spänningar som uppmätts vid överborrning. Största horisontella spänningen i borrhål KFM01B uppgår till 35 MPa redan på 250 m djup. Högre spänningar är troliga på större djup; de indirekta bevisen från denna studie tyder på att största horisontalspänningen är minst 40 MPa på 400 till 450 m djup. Förekomsten av ”core discing” på mätnivå 2 indikerar att denna spänningskomponent till och med kan vara högre på dessa djup.

Contents

1 Introduction

This report presents an evaluation of the three-dimensional overcoring stress measurements conducted in borehole KFM01B at the Forsmark site. The measurements were conducted in 2003–2004 and reported by /Sjöberg, 2004/. The evaluation described in this report comprised interpretation of the measurement data from a geological perspective, as well as additional investigations and analysis of the measurement data. The work presented, which is one of the activities within the site investigation at Forsmark, was performed according to Activity Plan AP PF 400-04-16 (SKB internal controlling document).

The KFM01B borehole was originally planned to 100 m depth, but was extended to 500.52 m borehole length to accommodate hydraulic characterization and rock stress measurements. The borehole is located at the first drilling site, DS1, as shown in Figure 1-1.

The borehole orientation was 268° with a dip of 79°, measured at the borehole collar. Another core hole, KFM01A, was located in very close proximity to KFM01B at the first drilling site. The orientation of KFM01A was 318° with a dip of 85° (measured at the borehole collar). The total length of this borehole was 1,001.45 m. The projection on the ground surface of the boreholes at drilling site DS1 is displayed in Figure 1-2.

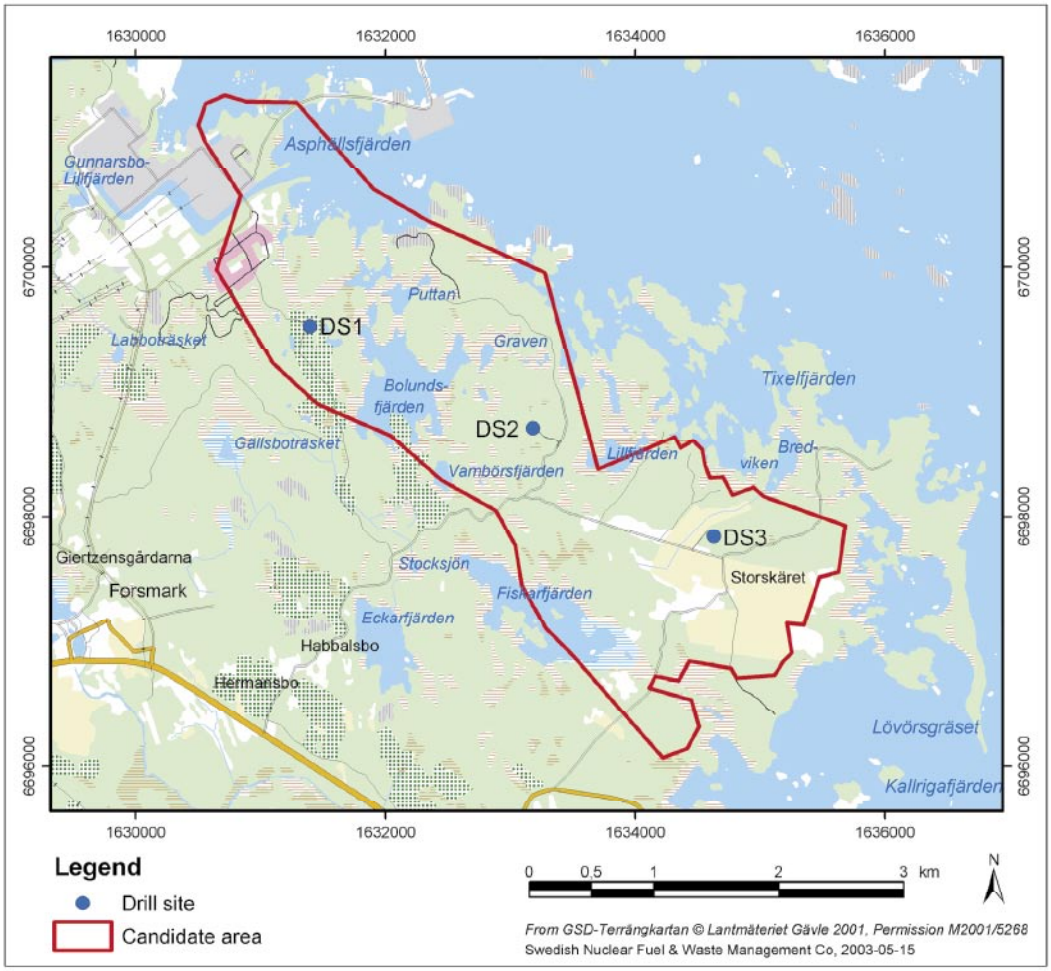

Figure 1-1. *Location of the first three drilling sites (DS1, DS2, DS3) within the Forsmark candidate area. Borehole KFM01B is located at drilling site DS1.*

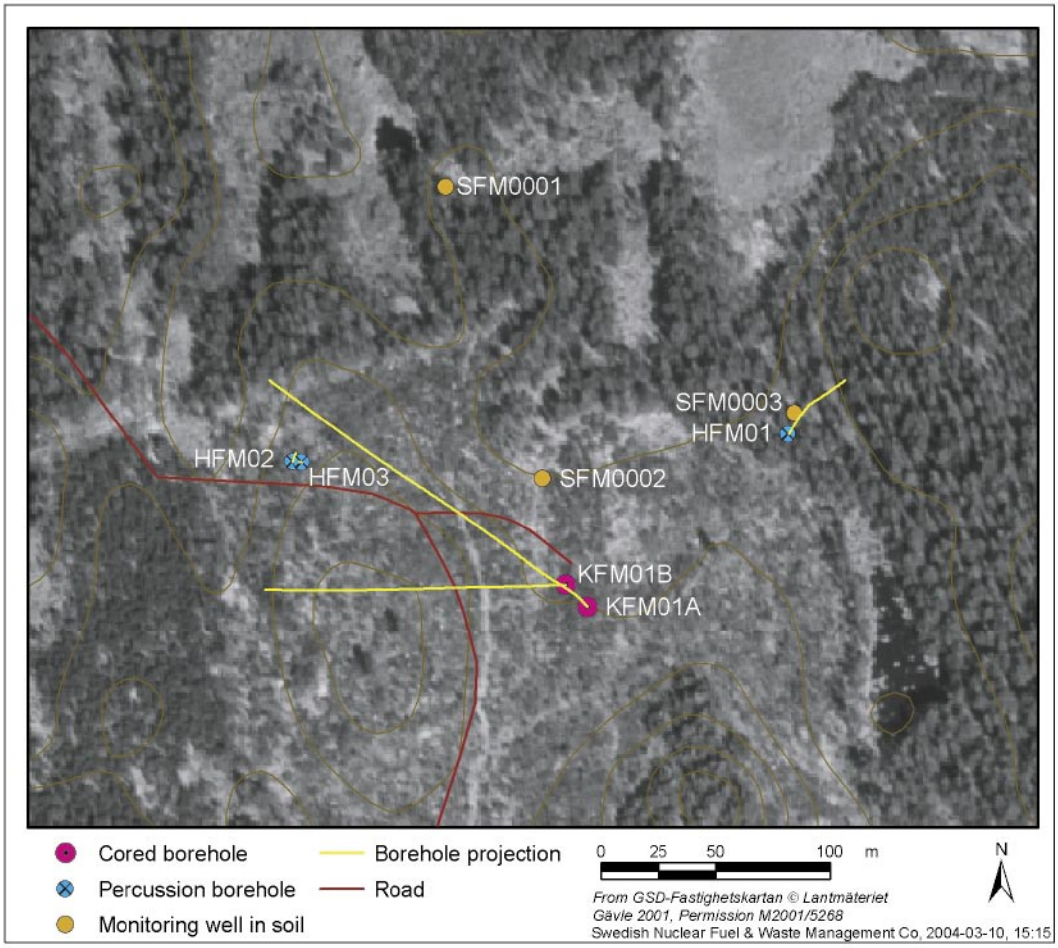

Figure 1-2. *Drilling site DS1 at Forsmark. Position and projection on the horizontal plane at the reference level (top of casing) of each borehole.*

2 Objective and scope

The objective of this work was to evaluate and interpret the overcoring stress measurement data from borehole KFM01B in a broader, geological-rock mechanics perspective. A secondary objective was to try to estimate the stress state from observed core discing and microcracking, to provide bounds on the measured stresses from the borehole.

The work included (i) comparison and correlation of geological data with measurement results, (ii) examination of core discing observations, (iii) examination of thin sections from a selected overcore sample to determine the extent of microcracking, and (iv) estimation of stress state from core discing and/or microcracking, as well as from P-wave velocity measurements from the nearby borehole KFM01A.

The geological data as well as core discing observations were obtained through geological mapping of the borehole /Berglund et al. 2004/ as well as from logging of the nearby borehole KFM01A /Petersson and Wängnerud, 2003/. Examination and mapping of microcracking of thin samples was conducted by staff at the Division of Rock Mechanics, Luleå University of Technology. Stress estimation from core discing was based on the work presented by /Hakala, 1999a,b, 2000/. Input data to this analysis included tensile strengths, which were obtained from preliminary results of tests conducted by Helsinki University of Technology on cores from the nearby borehole KFM01A /SKB, 2004a/. More extensive testing has been conducted on cores from several boreholes at the site, but these have not been made available to us (reports in press). Other pertinent geological and strength data was taken from the site descriptive model, version 1.1 /SKB, 2004a/.

The work also included programming of a computer code to calculate confidence intervals for rock stress measurement data, following an idea presented by /Walker et al. 1990/. The code was used to estimate the confidence of the resulting stress data from borehole KFM01B.

In this presentation, all stresses are denoted using a geomechanical sign convention with compressive stresses taken as positive. All stress orientations are given with respect to geographic north, using a right-hand rule notation.

3 Overcoring measurements in KFM01B

3.1 Overview and results

Overcoring stress measurements were conducted in borehole KFM01B, which was drilled from the ground surface with 76 mm diameter. All measurements were performed using the *Borre* probe /Sjöberg and Klasson, 2003/. Measurement procedure, interpretation, and final results are reported in /Sjöberg, 2004/. A total of 7 overcoring attempts were made on measurement Level 1, whereas 11 attempts were made on Level 2. Out of these, three and two tests, respectively, were considered successful for each level. The other tests failed – primarily due to extensive core discing of the overcored sample.

The results were evaluated using both classical analysis /see e.g. Amadei and Stephansson, 1997/ and transient strain analysis /inverse solution by Hakala et al. 2003/. However, the inverse solution of transient strain analysis could only be successfully applied in one case (test no 1:4:1). These results confirmed the stress magnitudes for the maximum horizontal stress obtained through classical overcoring analysis, but resulted in significantly lower values on the intermediate and minor principal stress, and, thus, also a lower vertical stress component. This finding lends further confidence to the measured stresses in the horizontal plane, and the inverse solution for pre-overcoring strains for test 1:4:1 was also used in place of the classical analysis results.

For two of the tests at Level 2, the transient strain analysis confirmed the magnitudes of the maximum horizontal stresses; however, the variation between the results for the presented coring advances in the pre-overcoring phase was large – thus, stresses cannot be said to be unequivocally determined through this analysis. The same was true, but even more pronounced, for all other tests, including those in which extensive core discing occurred; hence, these data could not be used with any confidence or in place of the classical analysis results. The final resulting stresses from both these analyses are presented in Table 3-1 and Table 3-2, and shown in Figure 3-1 (with an explanation given in Appendix C).

Table 3-1. Magnitudes and orientations of principal stresses as determined from overcoring and transient strain analysis (marked * and in *italic*) in borehole KFM01B.

Test no	Hole length (m)	Magnitude and trend/plunge of principal stresses					
		σ_1 (MPa)	(°)	σ_2 (MPa)	(°)	σ_3 (MPa)	(°)
*1:4:1 *)*	*238.94*	*41.3*	*104/06*	*21.9*	*198/34*	*6.9*	*006/55*
1:5:1		38.7	282/12	22.3	187/19	15.6	043/67
240.01							
1:7:1	242.05	40.2	289/12	32.4	195/17	19.0	053/69
Average Level 1 **)		39.5	283/05	25.4	191/25	14.6	024/64
2:3:1		42.3	141/28	25.2	030/34	10.3	261/43
412.79							
2:8:2	471.69	46.8	153/23	14.5	011/62	10.0	252/14
Average Level 2		44.1	150/24	19.7	035/43	10.7	261/37

*) data from transient strain analysis (inverse solution)
**) average based on inverse solution of 1:4:1 and classical analysis of 1:5:1, 1:7:1

Table 3-2. Horizontal and vertical stress components calculated from principal stresses from overcoring and transient strain analysis (marked * and in *italic*) in KFM01B.

Test no	Hole length (m)	σ_H (MPa)	σ_h (MPa)	σ_v (MPa)	Trend σ_H (°)
*1:4:1 *)*	*238.94*	*41.0*	*17.1*	*11.9*	*103*
1:5:1	240.01	37.7	21.6	17.4	103
1:7:1	242.05	39.4	31.1	21.1	114
Average Level 1 **)		39.3	23.4	16.8	105
2:3:1	412.79	37.2	18.6	21.9	152
2:8:2	471.69	41.7	10.4	19.3	157
Average Level 2		39.4	14.5	20.6	155

*) data from transient strain analysis (inverse solution)
**) average based on inverse solution of 1:4:1 and classical analysis of 1:5:1, 1:7:1

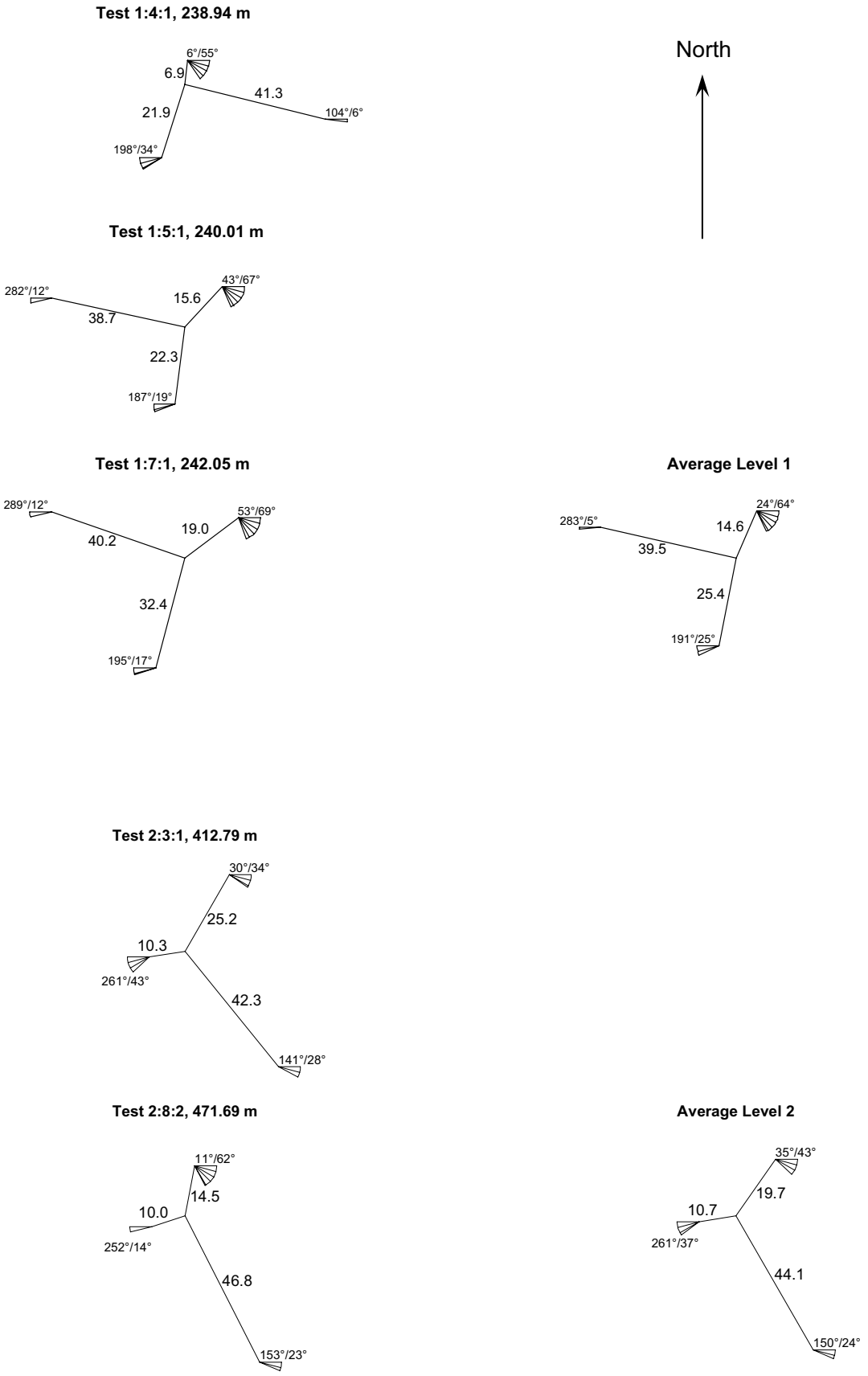

Figure 3-1. *Magnitudes and orientations of measured principal stresses in borehole KFM01B (see Appendix C for full explanation).*

3.2 Confidence intervals

The confidence intervals for the presented results were calculated using the methodology proposed by /Walker et al. 1990/, using a newly developed computer code. The code is described in Appendix A. Confidence intervals were determined for both the magnitudes and the orientations of the principal stresses at each measurement level. Using the data in Table 3-1, the 90%-confidence intervals for σ_1, σ_2, and σ_3 are presented in Table 3-3, Figure 3-2, and Figure 3-3. The confidence intervals for the horizontal and vertical stress components (σ_H, σ_h, and σ_v) are shown in Table 3-4, Figure 3-4, and Figure 3-5.

The confidence limits are fairly close to the average values, in particular for the major principal stress and the maximum horizontal stress component. Deviations are much larger for the intermediate and minor principal stress, as well as for the minimum horizontal stress and the vertical stress components (in terms of magnitude). Stress orientations are, however, relatively well constrained for all principal stresses, as the orientation of individual measurements are encompassed within the 90%-confidence limits.

Table 3-3. Calculated confidence intervals (90%) for the principal stress determined from overcoring stress measurements in borehole KFM01B.

Level		Magnitude and trend/plunge of principal stresses					
		σ_1 (MPa)	(°)	σ_2 (MPa)	(°)	σ_3 (MPa)	(°)
Level 1	Average	39.4	283/06	25.4	191/25	14.6	024/64
	90% lower	38.0	*)	16.1	*)	2.1	*)
	90% upper	44.0		36.6		23.1	
Level 2	Average	44.2	150/25	19.7	035/43	10.7	261/37
	90% lower	38.3	*)	10.6	*)	2.6	*)
	90% upper	51.5		34.9		10.9	

*) all orientation data are presented in Figure 3-2 and Figure 3-3

Table 3-4. Calculated confidence intervals (90%) for the horizontal and vertical stress components determined from overcoring stress measurements in borehole KFM01B.

Level		σ_H (MPa)	σ_h (MPa)	σ_v (MPa)	Trend σ_H (°)
Level 1	Average	39.3	23.4	16.8	105
	90% lower	37.3	12.8	6.6	*)
	90% upper	42.3	32.9	27.2	
Level 2	Average	39.4	14.5	20.6	155
	90% lower	32.2	6.1	11.1	*)
	90% upper	474.	21.5	30.2	

*) all orientation data presented in Figure 3-5.

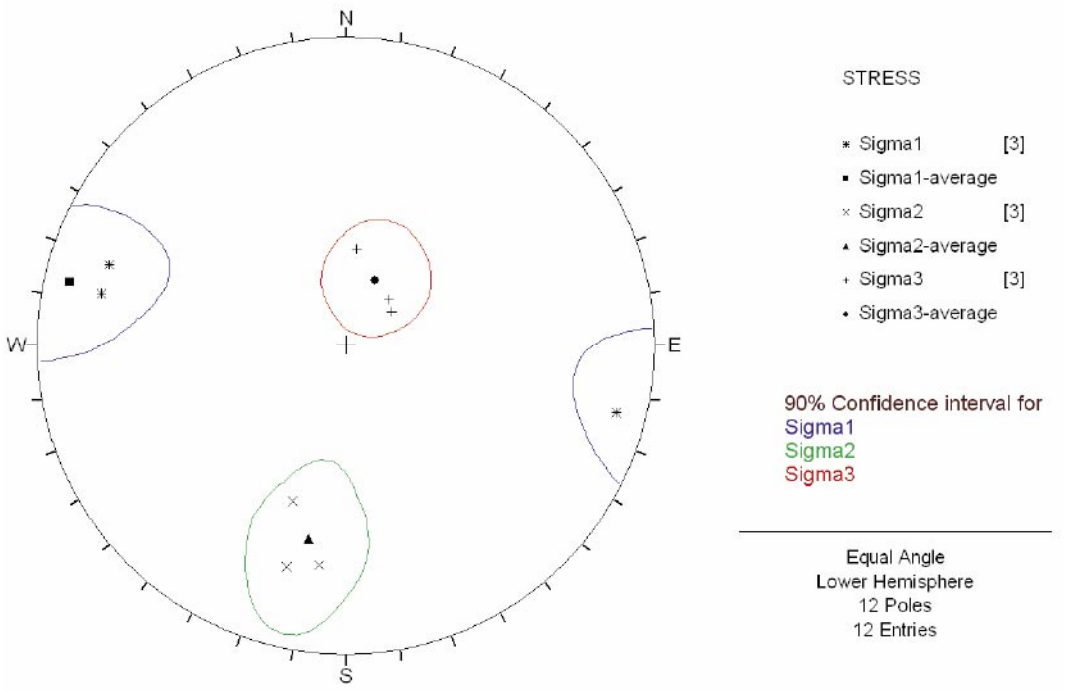

Figure 3-2. *Calculated confidence intervals (90%) for the orientation of the major principal stresses, σ_1, σ_2 and σ_3, at Level 1 in borehole KFM01B, shown in a lower hemisphere projection.*

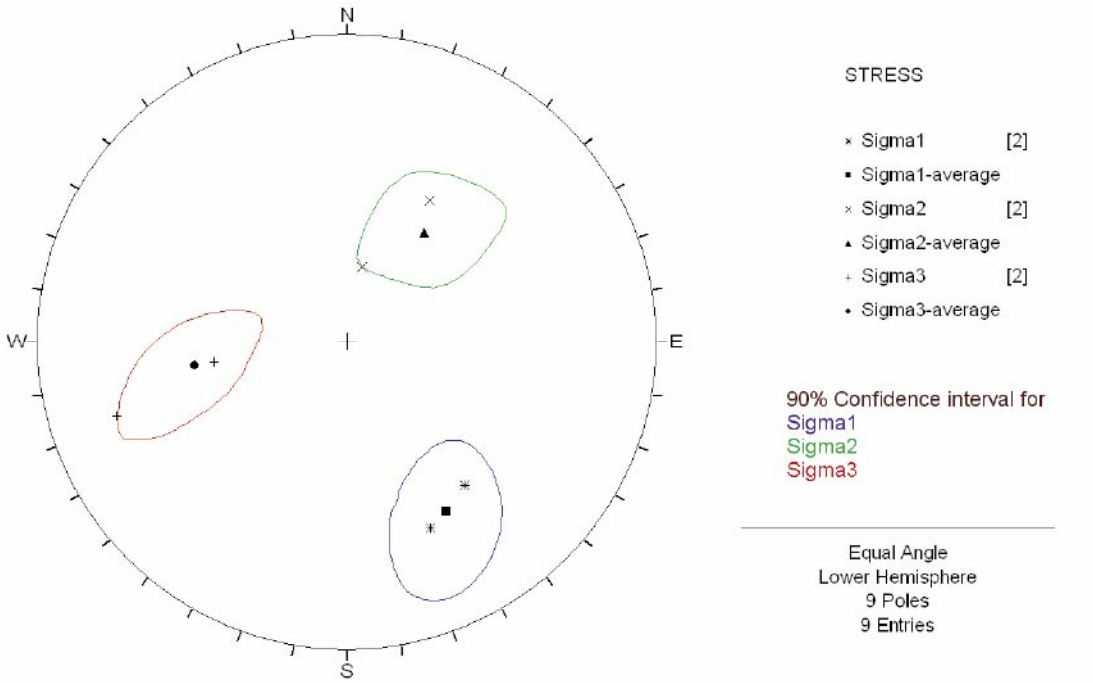

Figure 3-3. *Calculated confidence intervals (90%) for the orientation of the major principal stresses, σ_1, σ_2 and σ_3, at Level 2 in borehole KFM01B, shown in a lower hemisphere projection.*

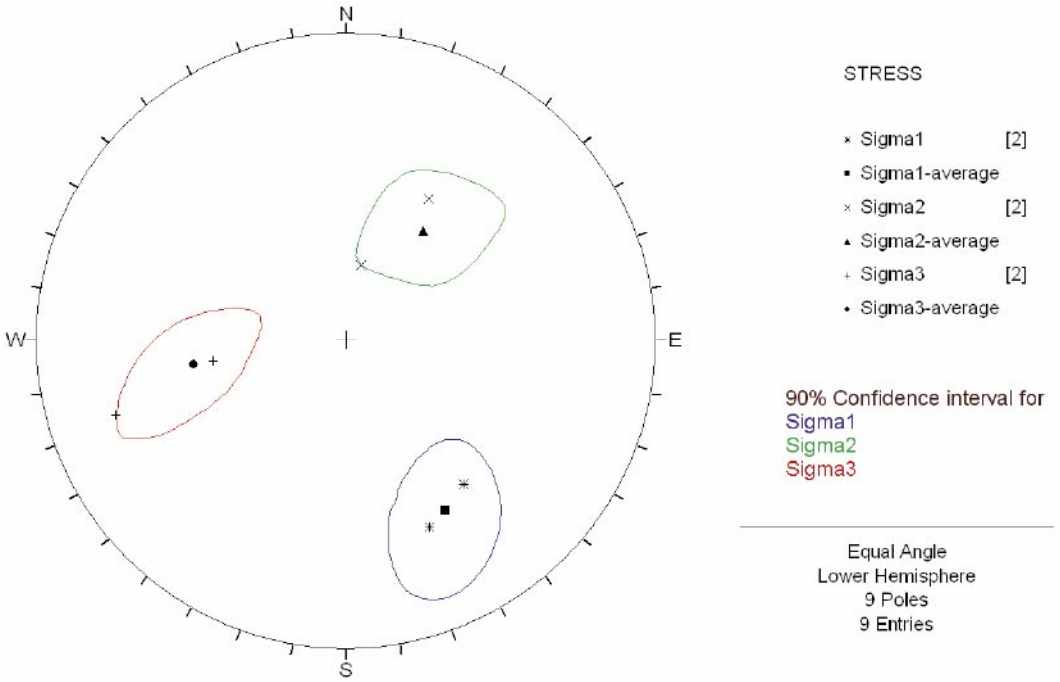

Figure 3-4. *Average values (■-markers) and 90%-confidence intervals (├──┤) for the horizontal and vertical stress components, shown together with measured values using overcoring for each measurement level (x-markers) in borehole KFM01B. (For the vertical stress, a line corresponding to the overburden pressure is shown for reference.)*

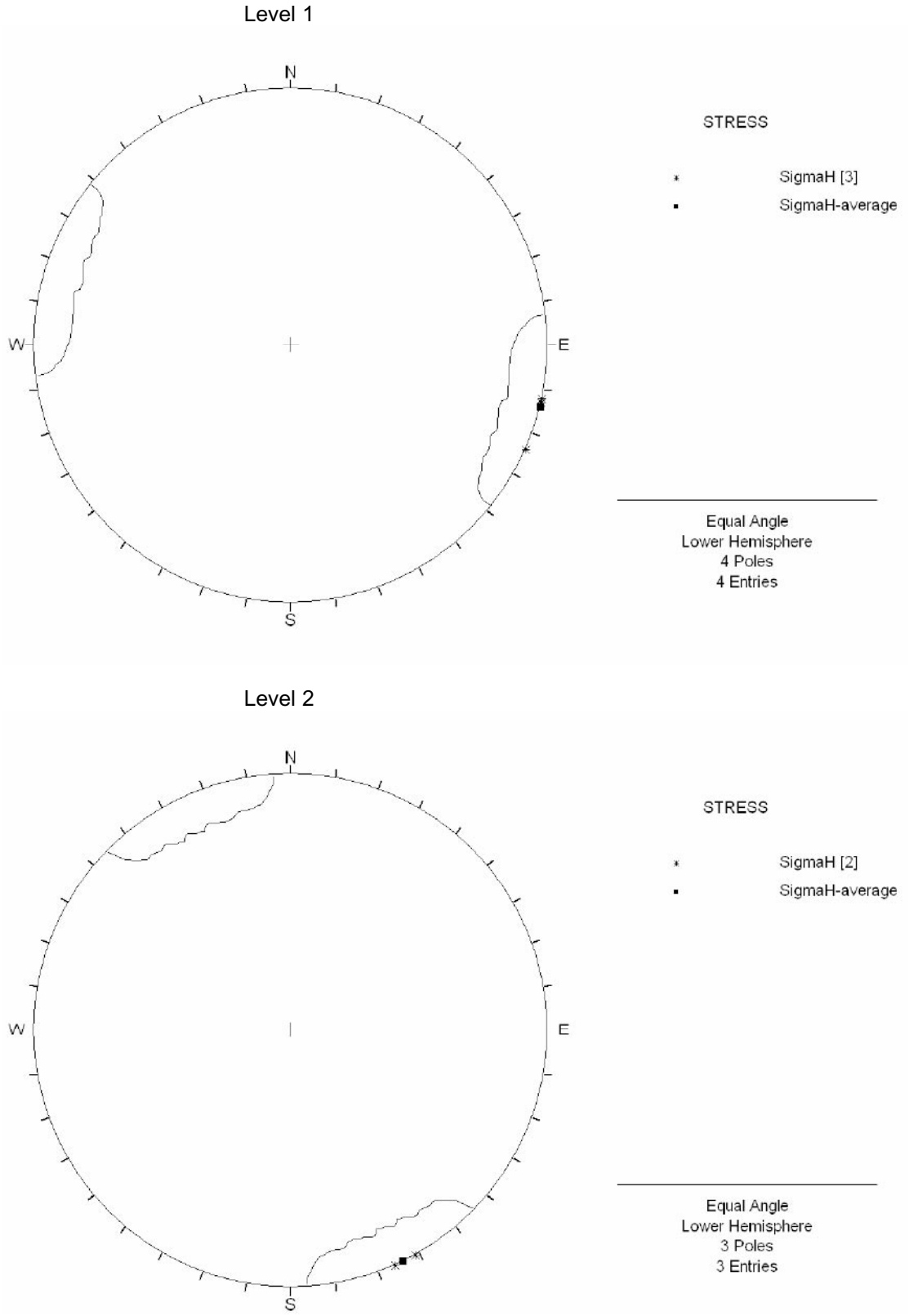

Figure 3-5. *Confidence intervals (90%) for the orientation of the maximum horizontal stress determined from overcoring measurements at Level 1 and Level 2 in borehole KFM01B.*

4 Examination of core damage

4.1 Core discing

4.1.1 Observed core discing

Core discing was observed in the overcore samples, with varying intensity, throughout the overcoring measurements. The extent and type of core discing was first mapped synoptically during the stress measurement campaign and complemented by measurements on photos of the overcore samples and associated core discing. Later, cores subjected to discing were mapped in more detail in conjunction with the geological logging of the core /Berglund et al. 2004; Berglund, 2004/.

In the following, the extent of core discing was determined based on both synoptic and detailed logging. The core discing geometry for each of the overcoring tests is summarized in Table 4-1 and Table 4-2. An example of observed core discing for one of the tests is shown in Figure 4-1. An average disc thickness could not be calculated, partly because the thickness of each disc can vary; neither could a reliable frequency distribution of disc thickness be compiled, as not all discs were measured (in detail) during geological logging. However, at Level 1, the majority of discs have thickness between 12–13 mm; thinner (< 12 mm) or thicker (> 13 mm) discs are much less represented. For Level 2, discs with thicknesses of 10 to 12 mm are in majority, but the variation in thickness is larger for this level.

Discing of solid (not overcored) core samples was only observed for a few cases – at 427.5 m borehole length, as well as between 431 and 433 m borehole length. The disc thickness was measured to 6 mm at 427.5, and 6 to 10 mm at 431–433 m borehole length /Berglund, 2004/, see also Table 4-2.

Table 4-1. Core discing geometry for overcoring tests in borehole KFM01B, Level 1.

Test no	Hole length (m)	Type of core discing	Geology	Disc thickness (mm)	
				Min	Max
1:1:1	235.89	Ring discing, lower portion	Granite to granodiorite, metamorphic, medium-grained, foliated.	10	12
1:2:1	237.02	None			
1:3:1	237.99	None			
–	238.69–239.65	Ring discing		18	18
1:4:1	238.94	None			
1:5:1	240.01	Ring discing, lower portion	Granite to granodiorite, metamorphic, medium-grained, foliated.	10	13
1:6:1	240.95	None			
1:7:1	242.05	None			
Level 1	Min and max			10	18

Table 4-2. Core discing geometry for overcoring tests in borehole KFM01B, Level 2.

2:1:3	406.92	Ring discing	Granite to granodiorite, metamorphic, medium-grained, lineated.	8	14
2:2:2	408.57	Ring discing	Granite to granodiorite, metamorphic, medium-grained, lineated.	8	15
–	411.63–413.84	Ring discing		15	20
2:3:1	412.79	Ring discing	Granite to granodiorite, metamorphic, medium-grained, lineated.	10	10
2:4:1	413.83	None			
–	413.47–414.82	Ring discing		9	9
2:5:1	415.16	Ring discing	Granite to granodiorite, metamorphic, medium-grained, foliated.	5	15
–	427.50	Core discing (solid core)		6	6
–	431–433	Core discing (solid core)		10	10
2:6:1	458.65	None			
–	458.71–460.12	Ring discing		11	11
–	461.80–463.21	Ring discing		8	8
2:7:3	465.05	Ring discing	Granite to granodiorite, metamorphic, medium-grained, foliated.	15	15
–	470.10–471.89	Ring discing		12	13
2:8:2	471.69	Ring discing	Granite to granodiorite, metamorphic, medium-grained, foliated.	10	15
2:9:1	472.98	None			
–	473.69–475.12	Ring discing		10	10
2:10:1	474.25	Ring discing	Granite to granodiorite, metamorphic, medium-grained, foliated.	8	15
2:11:1	475.34	Ring discing	Granite to granodiorite, metamorphic, medium-grained, foliated.	6	15
Level 2	Min and max			5	20

Figure 4-1. *Photo of observed core discing in overcore sample for stress measurement no 2:10:1 (474.25 m depth).*

4.1.2 Stress estimation from core discing

Information on core discing can be used to estimate the virgin stress state. A methodology for this was described by /Hakala, 1999a,b, 2000/. The methodology is based on the assumption that core discing is caused by pure tensile failure. Furthermore, continuous, homogeneous, linear-elastic and isotropic conditions (up to the point of failure) must be assumed. /Hakala, 1999a/ described both a computer program for analysing core discing and the acting stresses, as well as nomograms for quick assessment of the stress state. The nomograms have the following limitations (compared to the computer code):

- one principal stress must be aligned with the borehole;
- poisson's ratio must be 0.25; and
- the stress ratio σ_h / σ_H must be 0.25, 0.50, 0.75, or 1.0.

According to /Hakala, 1999a/, an accurate determination of the stress state requires information on core discing both from normal coring and overcoring (hollow core; ring discing). Also, the numerical model used for developing the methodology had fairly large zones, resulting in inaccurate results for thin discs /spacing of 10 mm or less; Hakala, 2004/. In borehole KFM01B all observed core discing was of the type ring discs (hollow core), with a few exceptions as noted above. Based on these uncertainties, as well as the sparse information on core discing geometry available, it was not deemed justifiable to use the numerical code. Hence, only the nomograms were used in the following preliminary stress estimation.

Indirect tensile tests on samples from the nearby borehole KFM01A have been determined in two test campaigns /Eloranta, 2004; Jacobsson, 2004/. Direct tensile strength test data are not available for the site. It should be noted that the indirect tensile strength may be different from that determined from direct tensile tests. However, the indirect testing configuration may actually more closely reflect the tensile strength governing core discing. Furthermore, given the inherent uncertainties in using the nomograms for stress estimation (as described above), the possible differences in direct and indirect tensile strength values are judged to be of relatively lesser importance.

The results of the indirect tests were used to assess the tensile strength of the rock in borehole KFM01B. These data indicated fairly consistent results with an average tensile strength of around 14 MPa and a standard deviation of about 2 MPa /Eloranta, 2004; Jacobsson, 2004/. Consequently, a value of σ_t = 14 MPa was used in the following.

Nomograms for two different σ_h/σ_H-ratios were used for each of the two measurement levels. Based on the overcoring results (Table 3-2), σ_h/σ_H was determined as 0.69 for Level 1 and 0.32 for Level 2. Thus, the nomograms for σ_h/σ_H-ratios of 0.50 and 0.75 were applied for Level 1, and 0.25 and 0.50 for Level 2, respectively. To estimate the in situ stresses, the ratios σ_t/σ_H and σ_v/σ_H are used together with the observed spacing of core discing. These two ratios are dependent on each other; hence, the maximum horizontal stress cannot be determined directly. Using the nomograms, a trial value was first determined for σ_t/σ_H from observed disc spacing. This value was then used to determine a corresponding value on σ_v/σ_H. The value on the maximum horizontal stress, σ_H, was calculated from both these ratios and compared. If the values differed, a new trial value was chosen and the procedure repeated until the value of σ_H converged. An example is shown in Figure 4-2 where 13 mm disc thickness yields a value of 0.41 for the ratio σ_t/σ_H and a value of 0.19 for σ_v/σ_H.

The obtained results for both measurement levels are presented in Table 4-3. For Level 1, the thinnest disc is set to be 10 mm and thickest to be 18 mm. For Level 2, disc thickness varies between 5 mm and 20 mm. Furthermore, since the vertical stress seems to be overestimated from the overcoring stress results /see also Sjöberg, 2004/, a theoretical value corresponding to the overburden pressure ($\sigma_v = \rho g z$, where z is the average depth for each level) was used. For the thinnest discs (10 mm for Level 1 and 5–10 mm for Level 2) and for $\sigma_h/\sigma_H = 0.50$, values which were outside the boundary of the nomograms resulted; hence, the value of σ_H did not converge for these cases. The same occurred for the thickest discs on Level 2 (18–20 mm) and σ_h/σ_H equal to 0.25 or 0.50. No stress estimate was thus possible for these cases and they were not included in Table 4-3.

For the other cases, the results showed that, using the maximum disc spacing, a lower boundary of the maximum horizontal stress is around 25–26 MPa magnitude for Level 1 and between 30 and 35 MPa for Level 2. For the most frequently observed disc thickness (12–13 mm on Level 1 and 10–12 mm on Level 2), the maximum horizontal stress is estimated to 33–41 MPa at Level 1, and at least 40–48 MPa at Level 2, possibly as high as 78 MPa.

For Level 2, the observation of discing of solid core can be used to further constrain the stress estimates. Assuming the overcoring would have led to ring discing at the same position with a disc thickness of 10 to 12 mm (most frequent for Level 2), nomograms for both overcoring and normal coring geometries can be overlaid /see Hakala, 1999a/. A stress estimate that matched both observations (overcore and solid core) could only be obtained when assuming that $\sigma_h/\sigma_H = 0.25$. The resulting maximum horizontal stress ranged from 30 to 90 MPa, depending on which combination of overcore and solid core geometry that was used. Interestingly, for 10 mm disc thickness for both core types, an unambiguous stress magnitude of $\sigma_H = 70$ MPa was obtained. Thus, it cannot be ruled out that the maximum horizontal stress can be as high as 70 MPa on Level 2.

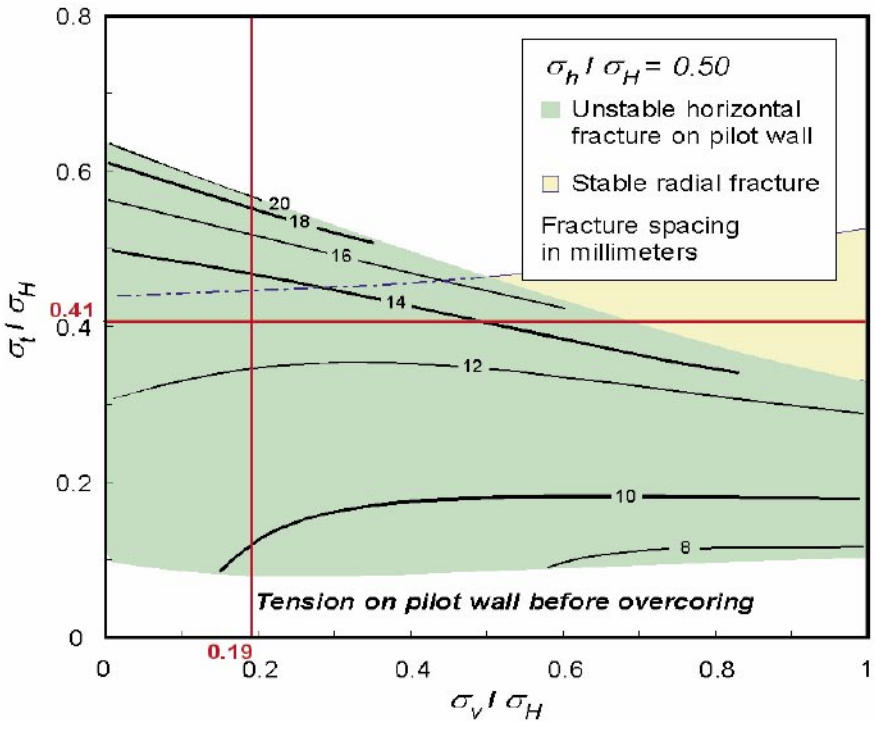

Figure 4-2. *Nomogram /from Hakala, 1999a/ for estimating in situ stress from observed core discing; example of procedure for Level 1, borehole KFM01B: disc thickness = 13 mm, σ_v = 6.3 MPa, $\sigma_h/\sigma_H = 0.50$, σ_t =14 MPa, yields $\sigma_t/\sigma_H = 0.41$, $\sigma_v/\sigma_H = 0.19$, from which $\sigma_H = 34$ MPa.*

Table 4-3. Stress estimation from core discing using nomograms by /Hakala, 1999a/ with the most common disc thickness marked with bold text.

Test level	$\sigma_v = \rho gh$ (MPa)	σ_h/σ_H	Disc thickness (mm)	σ_T/σ_H	σ_v/σ_H	σ_H (MPa)
Level 1	6.3	0.50	**12**	**0.34**	**0.15**	**41**
			13	**0.41**	**0.19**	**34**
			18	0.53	0.24	26
		0.75	10	0.14	0.06	100
			12	**0.39**	**0.16**	**36**
			13	**0.43**	**0.19**	**33**
			18	0.56	0.25	25
Level 2	11.7	0.25	5	0.13	0.11	108
			8	0.17	0.14	80
			10	**0.21**	**0.15**	**78**
			12	**0.29**	**0.24**	**48**
			15	0.40	0.34	35
		0.50	**12**	**0.35**	**0.29**	**40**
			15	0.47	0.39	30

The lack of solid core discing for the rest of the borehole indicates that stresses are not as high at these depths (assuming that the tensile strength is fairly constant). Using the nomograms of /Hakala, 1999a/, a very crude estimate may be obtained of the upper limit in terms of stress magnitude before the initiation of core discing. Although not completely conclusive, this indicates that the maximum horizontal stress is around 55 MPa (for a tensile strength of 14 MPa). The results are similar regardless of the chosen σ_h/σ_H-ratio.

Extensive core discing is not unusual in high stress environments. Examples can be found at e.g. URL /Martin and Stimpson, 1994/ and Hästholmen /Hakala, 2000/. The data from Hästholmen comprised disc thicknesses of between 8 and 13 mm, resulting in maximum horizontal stresses of between 30 and 50 MPa. Estimating the disc thickness from /Martin and Stimpson, 1994/ gave a thickness of between 5 and 10 mm, and a corresponding horizontal stress of 55 MPa. These stress estimates are in good agreement with the results of direct stress measurements conducted at each site. These findings lend some confidence to the method of stress estimation from core discing. It also appears that the values obtained for KFM01B at Forsmark are not unreasonable considering the discing geometry and the rock types at the site. However, the use of core discing to estimate in situ stress magnitudes is still a novel approach and calibration with additional field data is required. Therefore, these results must be used with caution and can only be considered as a guide when assessing the stress state for Forsmark.

4.2 Thin sections

Overcoring of test no 2:5:1 (415.16 m borehole length) in borehole KFM01B resulted in extensive core discing of the entire overcore sample. The strain record for this measurement is shown in Figure 4-3. A notable scatter is observed for strain rosette no 1 (gauge number 1, 2, 3) already after a few minutes of overcoring (corresponding to approximately 3 cm of coring advance). A closer examination reveals that the axial gauges show the largest discrepancy (compared to a typical strain response curve), starting approximately at 10:11 to 10:12. Additional scatter could be noted after approximately 10 cm of overcoring (at 10:14 in Figure 4-3) and for all strain gauges, thus indicating disturbances and incipient debonding prior to the drill bit reaching the strain gauge position (at 16 cm). These findings are further confirmed by the lack of the typical local maxima and minima in strain response at the gauge position. Rather, strains continue to increase or decrease until approximately 18 cm of overcoring (10:19) when they are clearly fully debonded and no longer functional. Signs of early debonding (prior to 16 cm coring advance) was even more pronounced for other tests on Level 2, e.g. 2:7:3, in which strain gauges ceased to function completely after only 5 cm of overcoring.

Since actual core discing is believed to occur once the rock is fully relieved from the acting stresses (through overcoring), the signs of disturbances prior to the drill bit having reached the strain gauge position are puzzling. A hypothesis was formulated as to whether the disturbances in the early, pre-overcoring, phase could be due to damages in the pilot hole wall itself. If the acting stresses are high enough, borehole damage (e.g. spalling-type failure in small scale) is possible due to the creation of the pilot hole. Such damages, if present, could be the reason for premature debonding of strain gauges. To test this hypothesis, a set of thin sections was prepared for test no 2:5:1. These were investigated with respect to microcracks and possible spalling-type failures around the pilot hole.

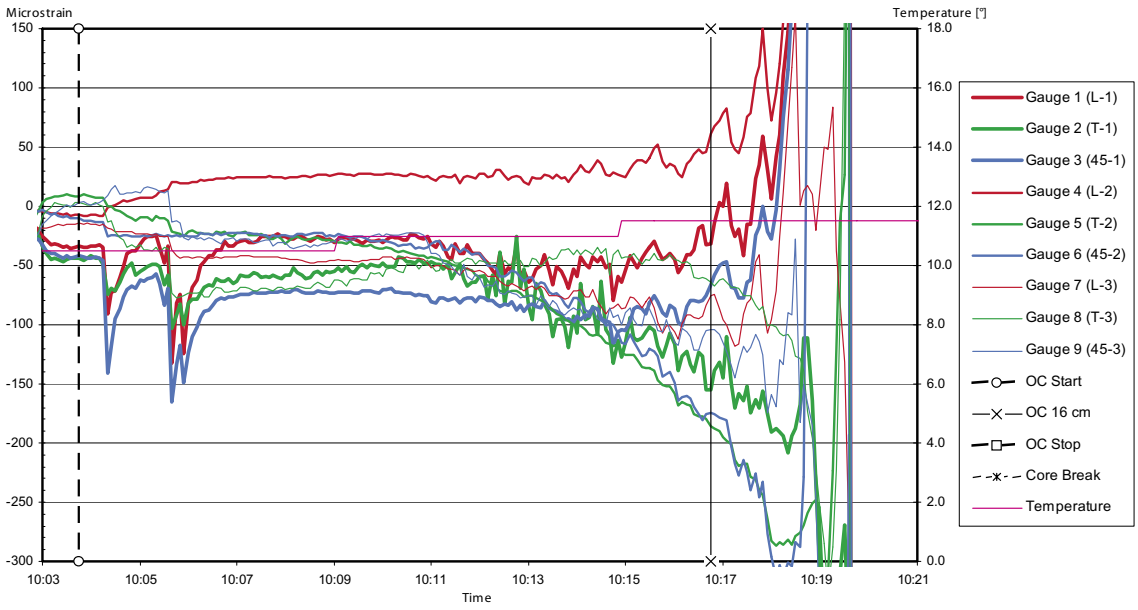

Figure 4-3. *Measured overcoring strain response for test no 2:5:1 in borehole KFM01B (strain values were reset to zero at 09:55).*

4.2.1 Preparation of thin sections

Thin sections were prepared for test 2:5:1 at 415.16 m borehole length. The sections were taken from one (disc-shaped) sample showing crack initiation, indicating that the sample was about to break into core discs (see Figure 4-4 and Figure 4-5). Micro cracks were mapped on thin sections, prepared from the sample, using the method from previous similar studies at Luleå University of Technology /Carlsson et al. 1999/.

In total, twelve thin sections were prepared from the overcore sample – six vertical and six horizontal, see Figure 4-6. Three of the vertical thin sections (labelled V1, V3, V5) were taken from the position where the strain gauge rosettes were glued onto the sample (120° between each other), see Figure 4-6a. Three of the vertical thin sections (labelled V2, V4, V6) were taken between the strain gauge positions (60° from the position of the glue and 120° between each other). The horizontal sections where taken between the upper surface and the existing crack, see Figure 4-6a. Three of the horizontal thin sections (labelled H1, H3, H5) were taken from the strain gauge position and the other three (labelled H2, H4, H6) were taken between these positions (60° from the position of the glue) (Figure 4-6b). The vertical and horizontal thin sections were numbered relative to each other i.e. V1 is positioned beside H1, etc.

It should be noted that the absolute orientation of the samples could not be determined, i.e. which of the sections V1, V3, V5, and H1, H3, H5, that corresponded to each of the three strain gauge rosettes, as the strain gauges had completely debonded when the overcore sample was retrieved.

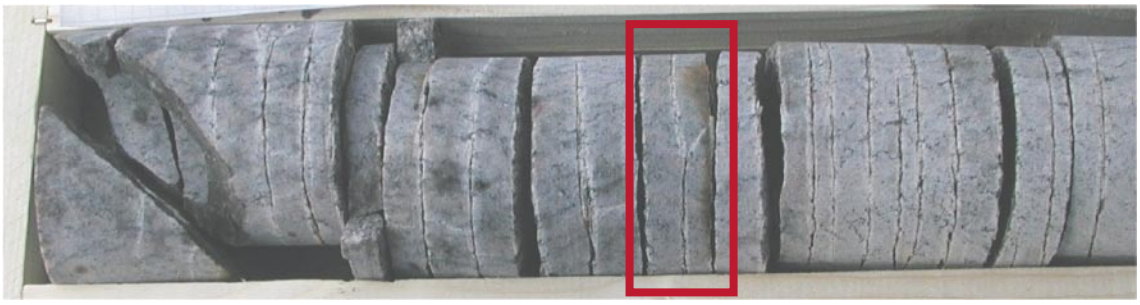

Figure 4-4. *Overcore sample from test no 2:5:1,with the rock sample used for thin section preparation marked with a red rectangle.*

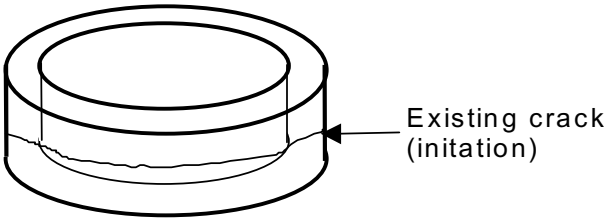

Figure 4-5. *Crack initiation in a sample subjected to core discing during stress measurement no 2:5:1 (415.16 m depth).*

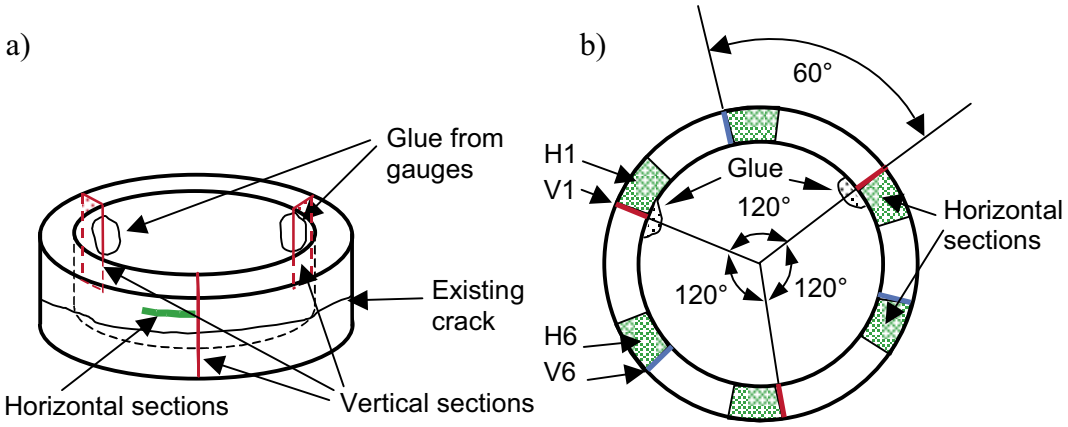

Figure 4-6. *Illustrations showing from where on the sample the thin sections were prepared.*

The thin sections consist of a thin glass slide onto which a very thin slice (0.3 µm) of rock is glued. The section is treated with a fluorescent epoxy, which fills openings like cracks and pores, and when lit with ultraviolet light, the cracks are shown as lines and can hence easily be detected and characterised. The thin sections were thereafter studied in an optical microscope at 100 times magnification. The size of a thin section was 17–18 mm in height and 12 mm in width.

Lines were marked on the thin sections, as shown in Figure 4-7. For vertical thin sections, lines 1 through 3 are termed vertical lines, whereas lines 4 through 9 are termed horizontal lines. For horizontal thin sections, lines 1 through 3 are termed tangential lines and lines 4 through 6 are termed radial lines. Note that line 3 is located closest to the inner (pilot hole) surface for both types of thin sections. Along these lines, microcracks were systematically mapped with respect to fracture orientation, fracture length, and the number of fractures. The method is here called line mapping and is similar to the scanline survey or line sampling methods used in e.g. tunnel mapping. From the data gained during the mapping, a simplified model of the crack distribution in the sample was established.

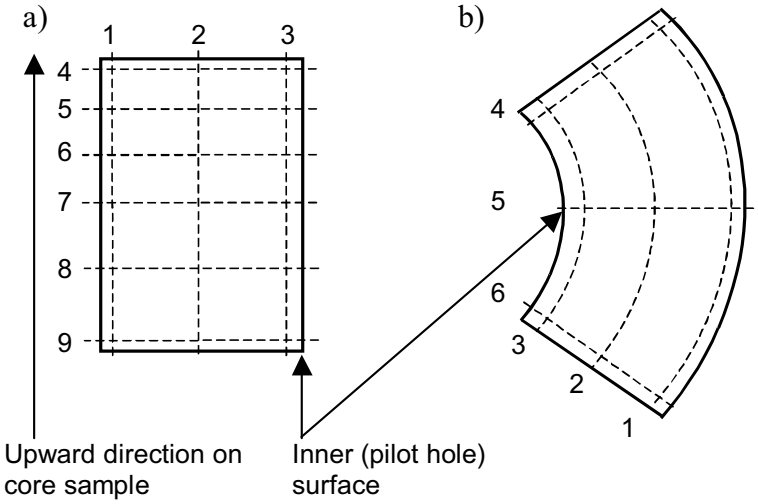

Figure 4-7. *The lines along which the thin sections were mapped: a) vertical thin sections, and b) horizontal thin sections (not to scale).*

4.2.2 Results from coarse examination of thin sections

In order to get a general view of the crack pattern within the rock samples, a coarse examination was first performed on the thin sections without counting any fractures. Only the larger microcracks (longer than 1 mm) were included in this examination.

For the vertical thin sections (V1–V6) there seems to be a higher amount of large (wide and long) microfractures close to inner boundary of the sample, i.e. close to, or crossing line 3 in Figure 4-7a, compared to the outer boundary of the sample (line 1 in Figure 4-7a). This is most evident for thin sections V1 and V6, less but still evident at thin sections V3 and V4, but not visible for thin sections V2 and V5. It was also observed, especially for thin sections V1 and V6, that the cracks along the inner boundary (line 3 in Figure 4-7a) of the sample, were parallel or inclined with a small angle to the boundary, i.e. being tangential to the inner boundary. A photo of a vertical thin section showing a tangential fracture is shown in Figure 4-8.

The microfracture parallel to the inner boundary shown in Figure 4-8, has a length of approximately 8 mm (entire fracture not shown in photo), and follows the boundary of the thin section. Close to the larger horizontal fracture (core discing fracture) the tangential fracture deviates and follows the horizontal fracture. Several horizontal fracture splays can be noted from the vertical (tangential) fracture. The tangential fracture parallel to the pilot hole wall surface has a width of 0.01 mm, becoming slightly wider as it bends toward the horizontal fracture (0.01–0.02 mm). The large horizontal crack almost splitting the core has a width of about 0.1 mm (visible to the eye without microscope). The other, less extensive microfractures exhibit widths in the range of 0.005 to 0.01 mm.

For the horizontal thin sections (H1–H6), similar results where observed, with a larger amount of large (wide and long) cracks along the inner boundary (line 3 in Figure 4-7b) compared to the outer boundary (line 1 in Figure 4-7b). This was most evident for thin sections H1, H4, H5, and H6. The opposite was true for thin section H3. For thin section H2 there were no obvious differences between the inner and the outer boundaries.

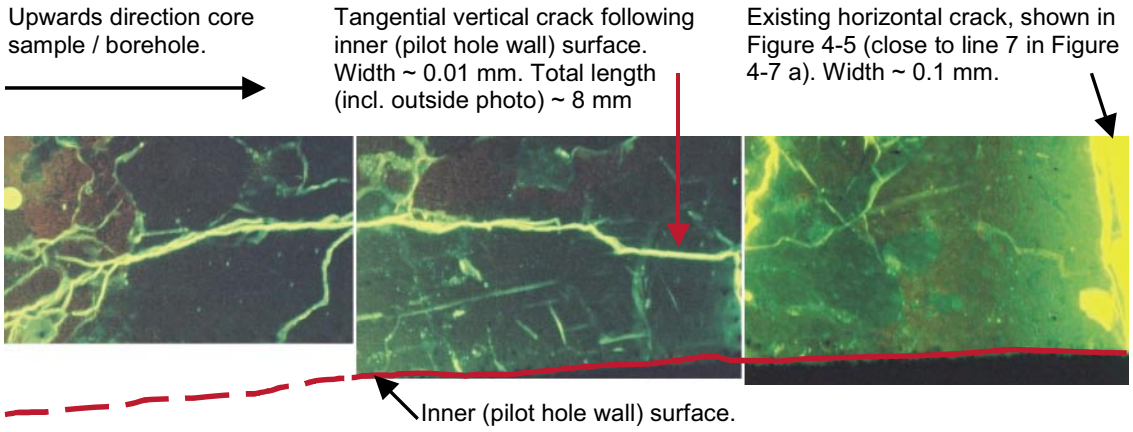

Figure 4-8. *Photos of thin section V6, from horizontal line 8 to horizontal line 7 (cf Figure 4-7a), following the inner (pilot hole) surface (line 3) and showing a large tangential crack parallel to the inner surface.*

Also, notable differences were observed when comparing the vertical and horizontal thin sections: (i) a higher density of cracks was observed on the vertical thin sections; (ii) the cracks on the vertical thin sections seemed to be larger (wider and longer); and (iii) all vertical thin sections contained one large crack extending from the inner to the outer edge, thus crossing the entire thin section. This is the same crack as the one observed on the overcore sample (cf Figure 4-6). Parallel to this large crack several smaller cracks were observed.

It should be noted that larger fractures located close to the boundary of the overcore sample may be underrepresented in the thin section examination. This is because the ends of the thin sections are damaged in the production of thin section.

4.2.3 Results from line mapping examination of thin sections

The line mapping of the thin sections was performed in order to verify and quantify the observations made by the coarse examination. Along each line the total amount of microcracks were mapped and the fractures were categorized in four directions – vertical, horizontal, and inclined 45° and –45°. For simplicity, microcracks inclined at +45° and –45° were treated as one group. The length of the microcracks was divided into three categories; shorter than 0.5 mm, between 0.5 and 1 mm, and longer than 1 mm. Consequently, the lime mapping provides some statistical data that complement the coarse examination, in which only the larger microcracks (longer than 1 mm) were included.

To be able to compare results, a ratio between the numbers of microcracks with a certain parameter (e.g. orientation or length) and the total number of microcracks mapped along a line, was calculated, since the amount of mapped microcracks along a line varies. The complete results are shown in Appendix B, and summarized in Figure 4-9 for the vertical thin sections. In this Figure, as well as in Appendix B, dotted lines with filled markers were used to show data from thin sections taken from the position where the strain gauge was attached to the sample (see Figure 4-6). Solid lines with open markers were used to show data from thin sections taken from the positions where there were no strain gauges attached to the rock.

The line mapping did confirm some of the observations from the coarse ocular examination of the thin section. The total amount of mapped micro cracks was always higher along line 3 (inner boundary) compared to line 1 (outer boundary) on all six vertical thin sections (V1–V6). For four of the six thin sections, the ratio of vertical microcracks was higher for line 3 than for line 1. The highest amount of long microcracks was found on line 1 in three cases and on line 3 in three cases. The same was found for the medium-long microcracks (see also Appendix B and Figures B1 through B6). The results of the line sampling showed, not surprisingly, that the amount of small fractures is much larger than the amount of large fractures.

From Figure 4-9, one can observe that the total number (summarizing the results from both vertical and horizontal lines) of mapped microcracks on thin sections V1, V3 and V5 are lower than for thin sections V2, V4 and V6. A higher ratio of vertical and horizontal microcracks was observed on thin sections V1, V3, and V5. Consequently, the opposite was observed for the inclined orientation, i.e. more on V2, V4, and V6. The majority of the mapped microcracks were shorter than 0.5 mm. The ratio of short microcracks seems to decrease on thin sections V1, V3, and V5, whereas the ratio of medium, and especially, long microcracks were higher. Naturally, the opposite was observed for thin sections V2, V4, and V6, i.e. more short microcracks compared to medium and long cracks.

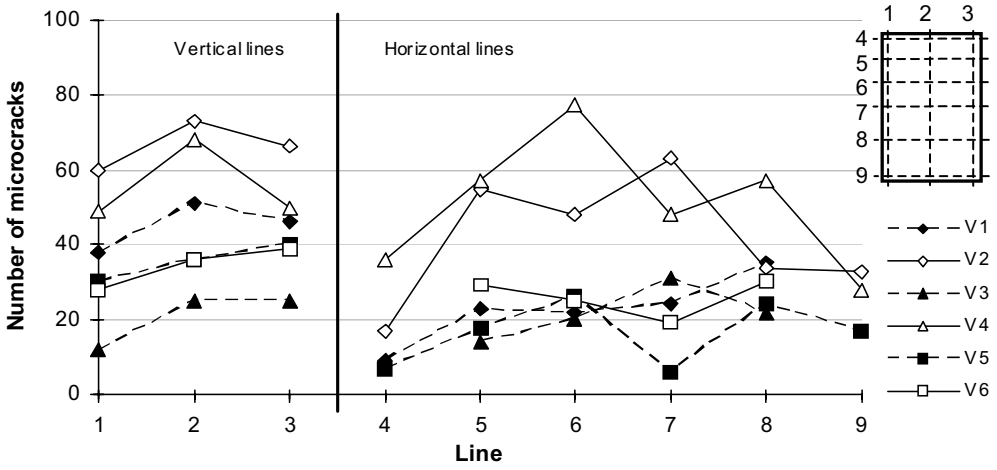

Figure 4-9. *Total number of microcracks along the nine lines (vertical lines 1 through 3; horizontal lines 4 through 9) on the vertical thin sections.*

Summarizing the number of horizontal fractures crossing vertical lines on the vertical thin sections over the length of the strain gauges used in overcoring measurements, gives an average of 5.5 microfractures per 10 mm of vertical length. The width of each microfracture was found to be between 0.005 and 0.01 mm; hence, the total fracture aperture is about 0.03 to 0.06 mm per 10 mm. This includes pre-existing microfractures (as these cannot be distinguished from cracks formed during drilling of the hole). These numbers correspond to an extensional strain of at least 2,700 µstrain. Given this high strain value, it is not surprising that the strain gauges cease to function when extensive microcracking and/or core discing occurs.

For the horizontal thin sections the same approach was used. However, to be able to compare the inner and outer line (since they have different lengths due to curvature), a parameter labelled crack density was introduced. The crack density is defined as the ratio between the amount of mapped microcracks and the length of the line mapped. In this case, line 1 was determined to be 22 mm and line 3 to be 13 mm. When comparing line 1 and 3 it was found that on four of six horizontal thin sections, line 3 (inner) had the highest crack density, i.e. more microcracks per length unit. The results for the other horizontal thin sections are consistent with the results from the vertical thin sections (see also Appendix B, Figures B7 through B12). For the horizontal thin sections, the majority of the microcracks are inclined (60–80%) and short (60–80%). However, there are no obvious differences between the different sections.

Examination of thin sections has previously been performed on cores from the Äspö HRL by Li (2001). A direct comparison is not possible, since both the position and size of the thin sections differ in that study, compared to the present one. However, a rough comparison indicates that the fracture frequency is relatively equal in the two studies.

4.2.4 Fracture frequency and sample orientation

As mentioned previously, the absolute orientation of the thin samples with respect to the borehole and/or geographic north, could not be determined. By summarizing the number of vertical and tangential fractures per 10 mm horizontal length of each thin section, an indication of the possible differences in fracture frequency with respect to circumferential location is obtained, see Figure 4-10. This comparison shows that the highest fracture

frequency was for thin section V4, which is located between two strain gauge positions, whereas the lowest fracture frequency was found for thin section V2. Hence, it appears the borehole damage is more evident in some orientations than in others. This is, in itself, an indication that pilot hole damage is present. For a circular borehole, the maximum and minimum stress concentrations occur at 90° angles from each other. Assuming that high fracture frequency occurs at the stress maxima, the maxima and minima with respect to fracture frequency could occur between some of the thin sections (as these are separated by 120° along the circumference of the core sample). Hence, it is difficult to state, from Figure 4-10, which of the positions that correspond to higher or lower virgin stress.

Assuming a stress state that corresponds to the average stress of Level 2, i.e. a maximum horizontal stress trending 155° (relative North), the maximum stress around the pilot hole would be at 245° and 65° bearing, respectively (perpendicular to the maximum stress). This is confirmed by transient strain analysis of test no 2:5:1 /described in Sjöberg, 2004/, which showed the maximum stress concentrations at a bearing of 237.5° (taking into account all three principal stresses). The recorded orientation of the Borre probe strain gauges in test no 2:5:1 was 165°, 45°, and 285°, for gauge rosettes no 1, 2, and 3, respectively. These orientations are shown schematically in Figure 4-11. This figure clearly shows that rosette no 2 would experience the largest stress, whereas rosette number 1 and 3 would be lower stressed. Furthermore, the other stress maximum would be for a thin section located in between the strain gauge positions, i.e. V2, V4, or V6.

It can now be assumed that the thin section with the highest fracture frequency (V4) is the one located close to the maximum stress area at around 240° bearing. V4 would thus have a bearing of 225°. This means that V1 would correspond to strain gauge no 2 (at 45° bearing). These two thin sections are also those with the highest fracture frequency in Figure 4-10. While not fully conclusive, the above analysis indicates that spalling-type (compressive stress-induced) failures are likely to have occurred in the pilot hole wall of test no 2:5:1.

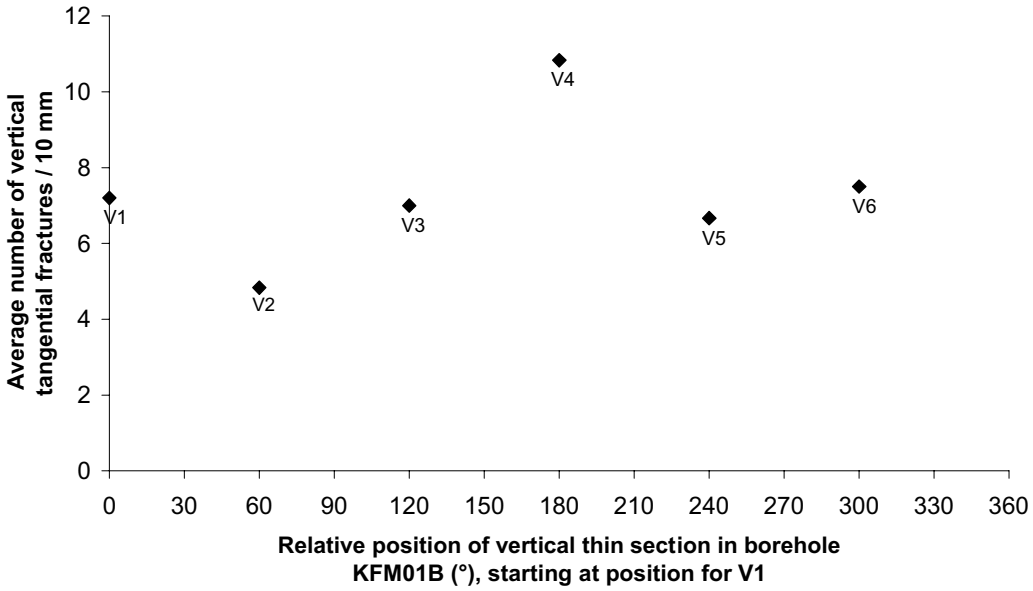

Figure 4-10. *Total number of vertical fractures crossing horizontal lines at all vertical thin sections. The position of the vertical thin sections is defined in degrees clockwise from the position of thin section V1.*

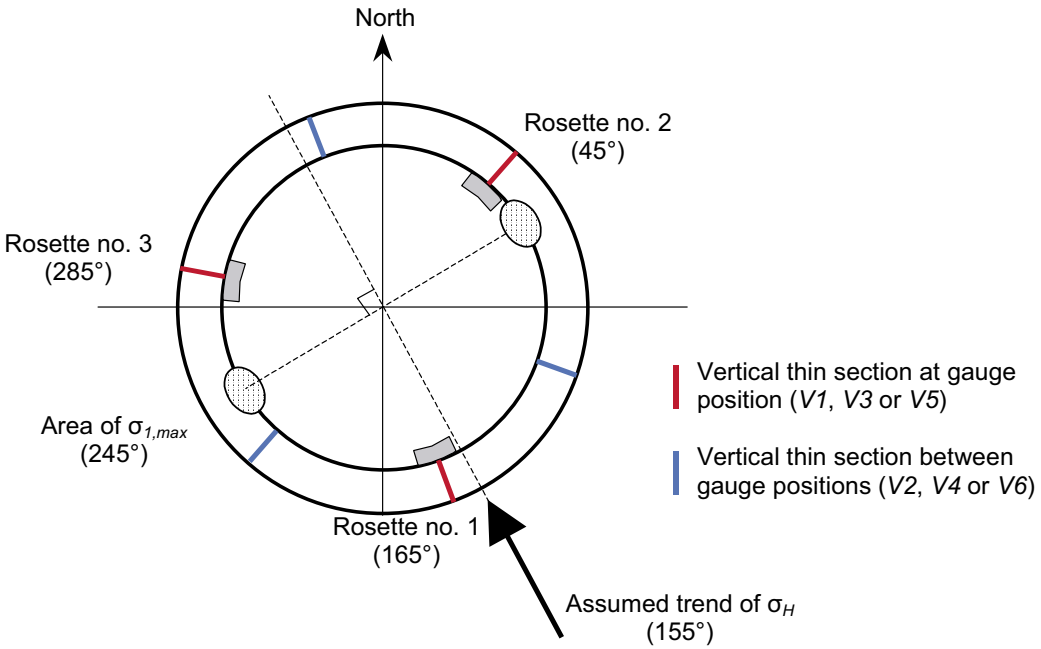

Figure 4-11. *Orientation of strain gauges of test no 2:5:1 shown together with the location of maximum stress concentrations in the pilot hole wall.*

4.2.5 Summary findings

Based on the examination of thin sections and the associated analysis the following can be concluded:

- Long, vertical fractures were observed on the vertical thin sections. These were oriented parallel to the inner (pilot hole wall) surface of the thin sections, thus being tangential to the pilot hole wall. The lengths of these fractures were up to 10 mm and normally terminated against horizontal (core discing) fractures. The presence of these tangential fractures is an indication of high tangential stresses around the pilot hole, and interpreted as initiating spalling failure of the pilot hole wall.
- The number and the total width of the horizontal (core discing) microcracks are sufficient to cause very large extensional strains over the strain gauge length used in overcoring measurements (10 mm). Thus, it is not surprising that the strain gauges cease to function when extensive microcracking and/or core discing occurs.
- A higher frequency of vertical fractures was found for certain circumferential orientations of the thin sections. This is an indication that borehole damage is more evident in some orientations than in others. Assuming a similar stress orientation as for the successful measurements on Level 2, the areas of maximum stress concentrations on the pilot hole surface can be tentatively linked to the thin sections with the highest fracture frequency. However, since the absolute orientation of the thin sections is not known (strain gauges had completely debonded when the overcore sample was retrieved), this conclusion cannot be fully verified. The analysis confirms, however, that spalling-type (compressive stress-induced) failures are likely to have occurred in the pilot hole wall of test no 2:5:1.

4.3 Stress estimation based on spalling failure

Using the indications from thin section mapping, it is likely that spalling failure in small scale has occurred. The phenomenon of spalling failure of brittle rock under high stresses is well-known. /Martin et al. 2001/ presented the following equation for describing the relation between the uniaxial compressive strength for intact rock and the principal stresses at failure:

$(\sigma_1 - \sigma_3) = K\sigma_c$,

where

σ_1 = major principle stress around the borehole,
σ_3 = minor principal stress around the borehole,
σ_c = uniaxial compressive strength of intact rock samples (laboratory-scale),
K = a constant, which depends on rock type.

/Martin et al. 2001/ stated that K ≈ 0.33, whereas /Diederichs, 2003/, /Diederichs et al. 2004/ and /Cai et al. 2004/ concluded that K could be as high as 0.60 for certain rock types and/or situations. Using data from laboratory tests on the granite from the Forsmark site /SKB, 2004b/, the uniaxial compressive strength was found to be σ_c = 224 ± 23 MPa (average ± standard deviation). Furthermore, the crack initiation stress for the granite was found to be 119 MPa. These values give K = 119/224 = 0.53. Using the above equations and the Kirsch solution for the stresses at the boundary of a circular opening, and setting σ_3 = 0 (at the boundary), the following relation can be derived:

$\sigma_h (3 - k) = K\sigma_c$

where

σ_H = maximum horizontal stress around the borehole,
k = σ_h/σ_H-ratio, and
K = a constant, which depends on rock type (K = 0.53 in this case).

Using the same σ_h/σ_H-ratio as for the core discing analysis (k = 0.25, 0.50, and 0.75), and σ_c = 224 ± 23 MPa, the resulting maximum horizontal stress was calculated, as shown in Table 4-4. The obtained values on the maximum horizontal stress (mean value) range from 43 to 53 MPa, depending on the assumed value on k.

Table 4-4. Calculated maximum horizontal stress from spalling failure.

σ_c (MPa)	K	k	σ_H (MPa)
224 ± 23	0.53	0.25	43 ± 4
		0.50	47 ± 5
		0.75	53 ± 5

4.4 Stress information from P-wave velocity measurements

P-wave velocity measurements on cores from KFM01A were conducted by NGI (Norwegian Geotechnical Institute) and reported in /Tunbridge and Chryssanthakis, 2003/. The results showed that the measured velocity down to 500 m depth had a consistent pattern with an anisotropy ratio between 1.0 and 1.1. The anisotropy ratio is here defined as the measured maximum velocity divided with the measured minimum velocity for a certain sample/depth. The maximum velocity varied between 5,400 and 5,700 m/s. Furthermore, the results from measurements below 500 m depth showed gradually reduced velocity and increase in the anisotropy ratio to 1.2.

Since all cores were non-oriented, the velocities were measured relative to the foliation orientation (in this case the strike of the foliation). The orientation of the maximum velocity was typically 160°–165° from the foliation direction and quite consistent with depth (measured clockwise looking down the hole). The definitions for these directions and planes are shown in Figure 4-12. The average foliation orientation is typically 175/78° (strike/dip) based on data in /Petersson and Wängnerud, 2003/, see also Figure 4-13. If the foliation direction (defined for the P-wave measurements) is taken to be the same as the strike of foliation, the typical orientation of the maximum velocity is 153° (333°). The orientation of the principal velocity is not well constrained mathematically at low anisotropy ratios. The error in the orientation of the principal velocities is probably in the region of ±10°–20° for cases when the anisotropy ratio is greater than 1.1, with larger errors below this limit /Tunbridge and Chryssanthakis, 2003/.

The velocity variation depends on both foliation orientation and induced microcracks in the core samples. An increased amount of microcracks resulting from stress relaxation from coring leads to lower P-wave velocities across the core. This would indicate that the maximum in situ stress is oriented perpendicular to the orientation of the maximum P-wave velocity, i.e. a trend of 063°(243°), which is nearly perpendicular to that measured in KFM01B. However, lower P-wave velocities also occur when measuring across the foliation direction. The data presented cannot be used to distinguish between these two effects; hence, no reliable stress orientation determinations can be made. The fact that foliation orientation may vary significantly from point to point and that measurements were only taken at fairly large intervals, only serve to add to the uncertainty in stress orientation determination from velocity data.

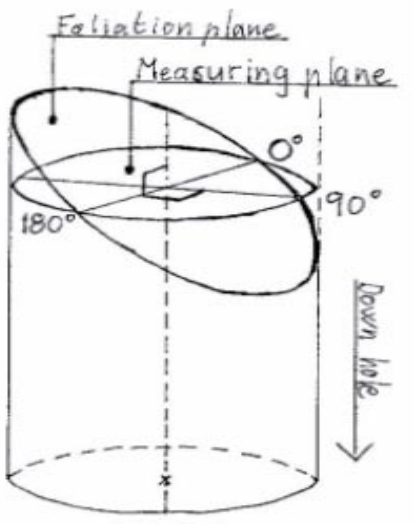

Figure 4-12. *Definitions of measuring plane and foliation plane for P-wave measurements /from Tunbridge and Chryssanthakis, 2003/.*

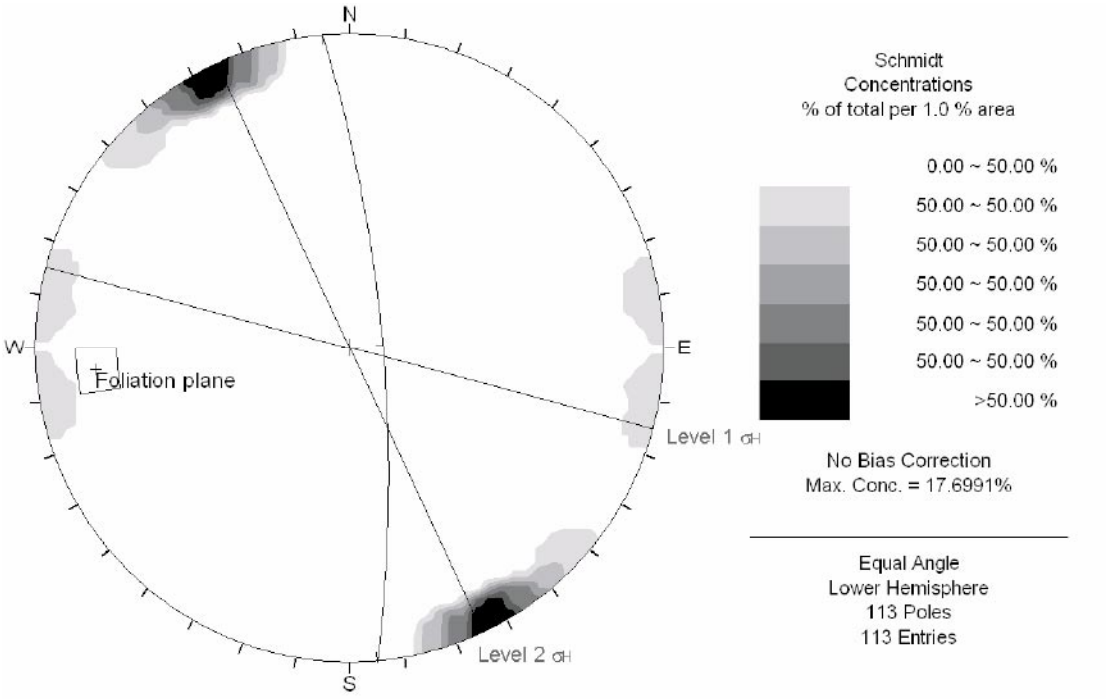

Figure 4-13. *Orientation of maximum P-wave velocity (grey-scale areas), average foliation plane orientation, and measured orientation of the maximum horizontal stress in KFM01B (Level 1 and Level 2).*

The possibility of core damage can be assessed from P-wave velocity measurements. Larger differences in principal stress magnitudes would result in larger differences in core damage due to the anisotropic stress relief that the core is subjected to. Hence, the measured anisotropy ratio can be used as a qualitative measure of the core damage potential. However, the P-wave velocity measurements from KFM01B indicated very small changes in anisotropy ratio down to 500 m, with no clear trends when comparing the different measurement levels for the overcoring measurements. Below 500 m, larger differences are noted. Both the maximum and the minimum P-wave velocities decrease and the anisotropy between them increase. This indicates larger disturbances of the cores (e.g. microcracking) but also larger differences in microcracking in different directions as a result of higher virgin stresses.

The P-wave data cannot be used to quantify the stress magnitudes; rather, they indicate that the stress magnitudes are high enough to cause damage to intact core samples at the depth where the anisotropy in P-wave velocity increases. Assuming that these stresses also cause spalling-type failure in the pilot hole wall /see e.g. Martin and Stimpson, 1994/, the stress magnitudes can be estimated in the same manner as that described in Section 4.3 above. Using the same values for the rock strength, this yields a maximum horizontal stress of 43–53 MPa at a depth of around 500 m.

It should be noted, however, that these P-wave measurements were only conducted in transverse orientation to the core axis. The largest amount of microcracking due to high horizontal stresses (in a vertical borehole) is expected in the axial (vertical) direction causing horizontal microcracks. This effect cannot be assessed using the reported test setup; rather, longitudinal measurements would be required.

4.5 Re-calculated stresses from overcoring measurements

The vertical stresses as inferred from the overcoring measurements were high in comparison to the normally accepted theoretical values with the vertical stress corresponding to the overburden pressure. The transient strain analysis presented in /Sjöberg, 2004/ confirmed that high tensile stresses develop in the axial direction during overcoring, leading to a high probability of tensile damage and microcracking of the overcore samples. This leads to overestimated strains in the axial direction, which, in turn, influences the value on the vertical stress component. All tangential strain gauges remain, however, almost unaffected by core damage in the axial direction (as confirmed by the transient strain analysis).

Assuming that the vertical stress corresponds to the overburden pressure ($\sigma_v = \rho g z$) the overcoring strains can be re-calculated to fit this value. Both the axial and inclined gauges need to be recalculated as both measure axial components of strain. The tangential gauges are not affected though. To obtain a lower vertical stress, the measured axial strains need to be reduced. Theory dictates that all axial gauge readings are equal; hence, these were first set to the same value for all three gauges (number 1, 4, 7). Theory states that the inclined strain gauges should be reduced by half of the value of the axial strain reduction /see e.g. Sjöberg and Klasson, 2003/. Since measurement scatter cannot be ruled out, it was decided to re-calculate stresses assuming a minimum and maximum value of $\sigma_v = \rho g z \pm 2$ MPa (with 2 MPa being the typical imprecision of the method, see /Sjöberg and Klasson, 2003/). Hence, strains were reduced (for all axial and inclined gauges simultaneously) until the vertical stress was in agreement with the above equation. Using the values in Table 3-1 and Table 3-2, the re-calculated stresses in the horizontal and vertical direction are shown in Table 4-5.

Table 4-5. Re-calculated horizontal and vertical stress components assuming that the vertical stress is equal to the overburden pressure, for borehole KFM01B.

Test no	Hole length (m)	Vertical depth (m)		σ_H (MPa)	σ_h (MPa)	σ_v (MPa)	Trend σ_H (°)
1:4:1	238.94	232.77	Min	35.7	24.5	4.2	117
			Mean	36.2	24.9	6.2	117
			Max	36.7	25.3	8.3	117
1:5:1	240.01	233.80	Min	34.5	19.2	4.2	104
			Mean	35.0	19.5	6.3	104
			Max	35.5	19.9	8.3	104
1:7:1	242.05	235.76	Min	35.5	27.9	4.2	117
			Mean	36.9	28.3	6.2	117
			Max	36.4	28.7	8.2	117
Average Level 1			Min	35.1	24.0	4.1	111
			Mean	35.6	24.4	6.2	111
			Max	36.1	24.8	8.3	111
2:3:1	412.79	399.18	Min	34.8	15.6	8.5	153
			Mean	35.2	16.1	10.5	153
			Max	35.6	16.5	12.5	153
2:8:2	471.69	455.15	Min	40.5	8.5	10.0	157
			Mean	40.8	9.0	12.1	157
			Max	41.2	9.5	14.1	157
Average Level 2			Min	37.6	12.1	9.2	156
			Mean	37.9	12.5	11.3	156
			Max	38.3	13.0	13.3	155

Comparing these values with the original stress data, a reduction of the vertical stress results in moderate changes to the horizontal stress components. The maximum horizontal stress magnitude decreases by 1–5 MPa, whereas the minimum horizontal stress is reduced by 1–3 MPa, with the exception of test no 1:4:1 in which an increase is obtained. The difference between the minimum and maximum values are (with the exception of the vertical stress component) small, typically less than 1 MPa. The stress orientations remain nearly the same after having reduced the vertical stress; a maximum change of 10° was found for test no 1:4:1. The same trends apply to the principal stresses (not shown here). The calculated average stresses for each Level are remarkably close to the original values (with the exception of the vertical stress component), the difference being only 1–2 MPa.

5 Correlation with geological data

5.1 Geology and rock types in borehole KFM01B

The geological information from borehole KFM01B stems from the detailed core logging reported by /Berglund et al. 2004/ and the draft RVS-model compiled by /Forssberg and Staub, 2004/. The rock mass in borehole KFM01B consists mainly of granite and granodiorite. Pegmatite is also found along the entire borehole length, with some larger areas at e.g. 280 to 320 m borehole length. Breccia occurs more sparsely and with the largest concentration between 78 and 84 m borehole length. Amphibolite is also sporadically present along the whole borehole, with the exception of the portion between 250 and 350 m hole length, where amphibolite is notably non-existent. Areas of amphibolite occur on both measurement levels for the overcoring measurements, in some cases fairly close to the test positions. The main distribution of rock types along the borehole is shown in Figure 5-1.

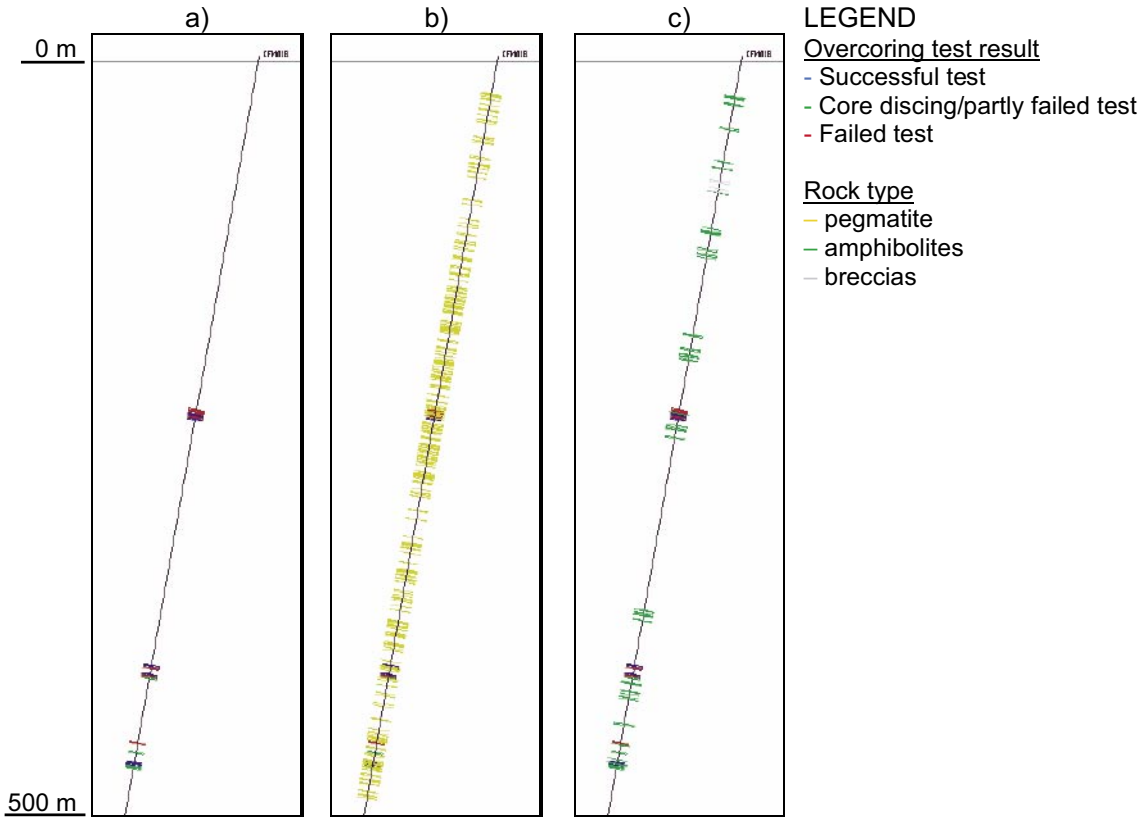

Figure 5-1. *Distribution of rock types in borehole KFM01B; figures from left: a) overcoring test positions, b) pegmatite, c) amphibolites and breccias. (Test positions from overcoring measurements are shown in each figure for comparisons.)*

Comparing the overcoring stress measurement results and the geological data, no clear correlations could be established between e.g. rock type and stress magnitude. The rock type at the position of each test (in the vicinity of the tests) is granite to granodiorite, metamorphic and foliated. The only difference is the grain size – at Level 1, grain size is medium coarse and at Level 2, grain size is fine to medium coarse. Pegmatite was present between the test positions, but no correlations could be found between e.g. failed tests and the presence of pegmatite. However, test no 2:9:1 (borehole length 472.98 m) was located very close to a pegmatite zone (as was noted already during logging of the overcore sample, /see Sjöberg, 2004/). For this test, no core discing was observed and the resulting stresses were significantly lower than for the other tests at Level 2.

Comparing borehole KFM01B with the nearby KFM01A /Staub, 2003/, it is found that the distribution of rock types is similar. Amphibolite occurs sporadically in both holes and it is not possible to link zones of amphibolite in the two boreholes with respect to overcoring test positions. Pegmatite is somewhat less frequent in borehole KFM01A compared to KFM01B, in particular for the upper 250 m. Below 400 m, the differences in the presence of pegmatite are small between the two holes.

5.2 Fractures in borehole KFM01B

In borehole KFM01B, the number of fractures is higher in the upper, 50 m, of the borehole. Also, the number of fractures is much less between 140 and 410 m borehole lengths, compared to the rest of the borehole. However, at 225 m borehole length, an increase in fracture intensity is noted, corresponding to the fracture density above 140 m depth. The same is observed for borehole lengths between 410 and 460 m, with the maximum fracture intensity occurring at 430 m length. The majority of these fractures are healed fractures. Overall, the fracture frequency is judged to be low to moderate for this type of crystalline rock.

The number of healed fractures is thus notably higher at Level 2 (compared to Level 1), see also Figure 5-2. The frequency of open fractures is also higher in the vicinity of the performed stress measurements on Level 2. In fact, the upper and lower groups of conducted measurements on Level 2 (412 and 472 m) are separated from each other by a zone with high frequency of open fractures, see Figure 5-2. The measurements on Level 1 were all taken in rock with very few open fractures (one of the few such sections along the borehole).

The planning of the overcoring measurements in borehole KFM01B relied, in part, on the RVS-model of the fractures in the nearby borehole KFM01A /Staub, 2003/. This first prognosis of the fracture conditions was only partly accurate, as fracture frequency was higher than expected between 415 and 458 m borehole length in KFM01B. Comparing the RVS-models from the two boreholes, there are large similarities regarding the frequencies of open fractures; however, perhaps not as large as could be expected considering the short distance between the two holes (Figure 5-3). The frequency of horizontal fractures is similar, but above 230 m hole length, there are more open horizontal fractures in KFM01B, compared to in KFM01A. On the other hand, a higher frequency of steep fractures (dip > 45°) is found in borehole KFM01A. Below 500 m hole length in KFM01A, the frequency of open fractures decreases, with the exception of a few limited sections. The fracture frequency in this portion of the borehole is considered low for this type of rock.

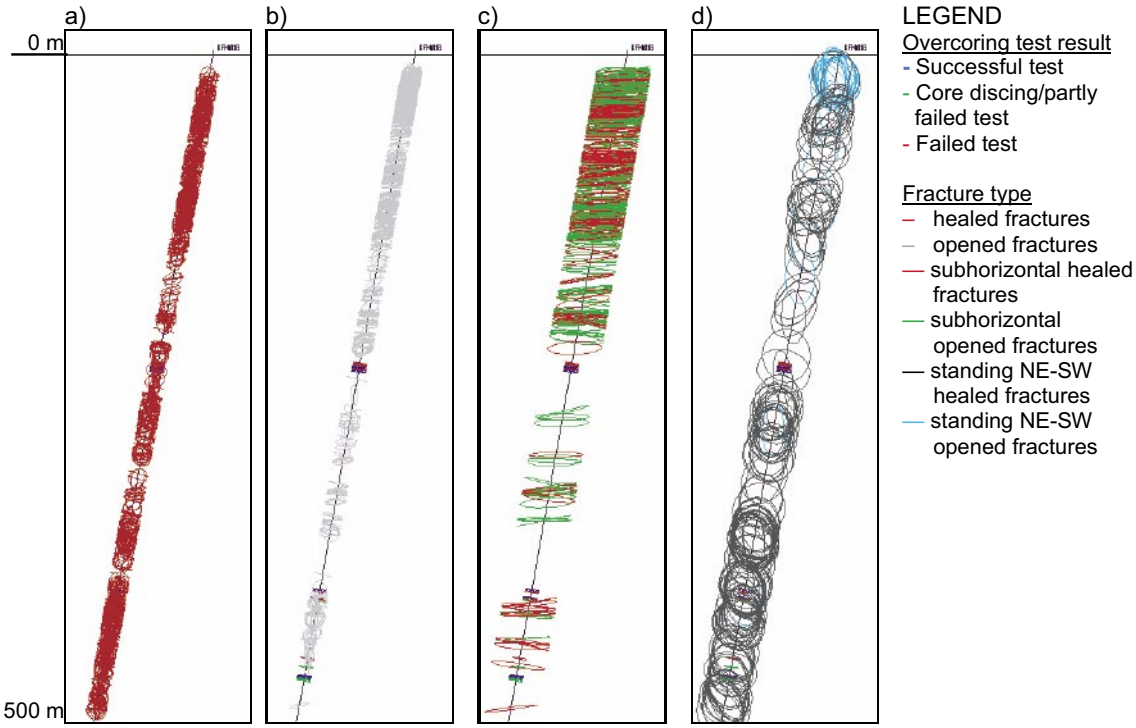

Figure 5-2. *Distribution of fractures in borehole KFM01B; figures from left: a) healed fractures, b) opened fractures, c) subhorizontal healed fractures and subhorizontal opened fractures, d) steeply dipping NE-SW healed fractures and steeply dipping NE-SW opened fractures. (Test positions from overcoring measurements are shown in each figure for comparisons.)*

The numbers of fractures and the determined RQD-value /SKB, 2004c/ for different distances from the overcoring measurement positions are shown in Table 5-1. Three intervals were considered: (i) from 16 cm above to 32 cm below the measurement point, (ii) from 1 m above to 1 m below the test location, and (iii) from 2.5 m above to 2.5 below the measurement point. The results showed that measurements on both levels were made in rock that is virtually free from fractures even on the 5 m-scale. This is particularly true for Level 1, but also applies to all the successful tests on Level 2. The fracture intensity in the vicinity of the measurements is, in general, slightly lower on Level 1 than on Level 2 as shown in Table 5-1.

It follows that the areas of intact, fracture-free rock, attract high stresses more easily than areas with a high frequency of fractures (in particular open fractures). This is under the assumption that a certain stress must be transferred through a (fairly large) volume of rock – areas with lower stiffness and/or lower strength would thus cause stress redistribution to areas with higher stiffness and/or strength within this rock volume.

For Level 1, large stress concentrations would result more or less exactly at the location where the measurements were taken. Such stress concentrations would also occur on Level 2, but to a much lower extent, since the fracture frequency is higher. This may explain why the measured stresses on both levels are similar in magnitude, despite the l arge differences in depth below surface.

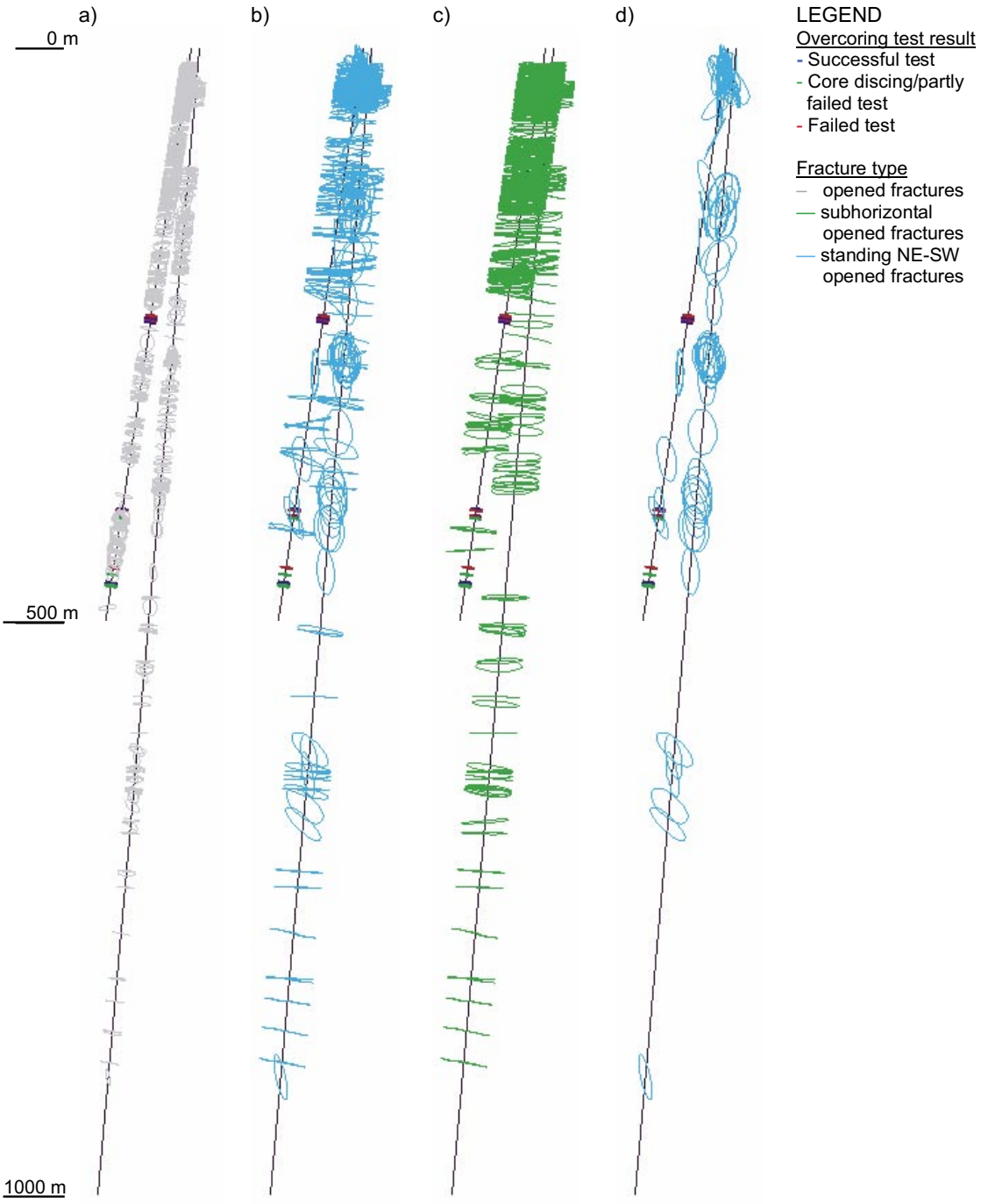

Figure 5-3. *Distribution of fractures in borehole KFM01B (500 m length) and KFM01A (1,000 m length); figures from left: a) all open fractures, b) all open NE-SW fractures, c) all open subhorizontal fractures (dip < 15°), d) all open steeply dipping NE-SW (dip > 45°) fractures. (Test positions from overcoring measurements are shown in each figure for comparisons.)*

Table 5-1. Fracture frequency and *RQD*-values for different intervals around the various overcoring measurement positions in borehole KFM01B.

Test no	Hole length (m)	OC-core (–16 to +32 cm) *)			Close (–1 to +1 m) *)			Far away (–2.5 to +2.5m) *)		
		Start–Stop	RQD	Fracture frequence**)	Start–Stop	RQD	Fracture frequence**)	Start–Stop	RQD	Fracture frequence**)
1:1:1	235.89	235–237	100.0	0	234–237	100.0	0.0	233–239	100.0	0.3
1:2:1	237.02	236–238	100.0	1	236–239	100.0	0.7	234–240	100.0	0.3
1:3:1	237.99	237–239	100.0	1	236–239	100.0	0.7	235–241	100.0	1.0
1:4:1	238.94	238–240	100.0	0	237–240	100.0	0.7	236–242	100.0	1.3
1:5:1	240.01	239–241	100.0	2	239–242	100.0	2.0	237–243	100.0	1.7
1:6:1	240.95	240–242	100.0	3	239–242	100.0	2.0	238–244	100.0	1.3
1:7:1	242.05	241–243	100.0	2	241–244	100.0	1.3	239–245	100.0	1.3
2:1:3	406.92	406–408	92.0	9	405–408	98.5	7.3	404–410	98.2	7.7
2:2:2	408.57	408–409	100.0	2	407–410	97.3	8.7	406–412	97.8	6.0
2:3:1	412.79	412–414	100.0	0	411–414	100.0	0.7	410–416	100.0	3.0
2:4:1	413.83	413–415	100.0	3	412–415	100.0	2.0	411–417	98.0	7.7
2:5:1	415.16	415–416	100.0	10	414–417	96.0	14.7	412–418	97.0	9.7
2:6:1	458.65	458–459	100.0	4	457–460	99.7	7.3	456–462	99.8	8.7
2:7:3	465.05	464–466	100.0	5	464–467	100.0	6.0	462–468	98.0	7.3
2:8:2	471.69	471–473	100.0	2	470–473	100.0	2.0	469–475	100.0	1.7
2:9:1	472.98	472–474	100.0	2	471–474	100.0	1.3	470–476	100.0	1.7
2:10:1	474.25	474–475	100.0	0	473–476	100.0	1.3	471–477	100.0	1.7
2:11:1	475.34	475–476	100.0	4	474–477	100.0	2.0	472–478	100.0	4.3

*) Rounded up/down to the nearest meter.
**) Numbers of fractures per meter.

6 Discussion and conclusions

A summary of the obtained stress estimates for borehole KFM01B is shown in Table 6-1. Only the horizontal and vertical stress components are shown here, as the principal stresses could not be determined from all the employed methods. However, the overcoring data indicate that the major principal stress is nearly horizontal; thus, the use of horizontal and vertical components for comparative purposes is justified. The stress estimates calculated from core discing and spalling failure observations are lower limits to the actual stress state.

Table 6-1. Best estimates of the horizontal and vertical stress components in borehole KFM01B inferred from measurements and analyses.

Level	Vertical depth (m)	Method	σ_H [MPa)	σ_h [MPa)	σ_v (MPa)	Trend σ_H (°)
Level 1	233–236	Overcoring data	39.3	23.4	16.8	105
		Core discing	33–41	–	–	–
		Spalling	–	–	–	–
		Re-calculated overcoring ($\sigma_v = \rho gz$)	35.6	24.4	6.2	111
Level 2	399–455	Overcoring data	39.4	14.5	20.6	155
		Core discing	40–48	–	–	–
		Spalling	43–53	–	–	–
		Re-calculated overcoring ($\sigma_v = \rho gz$)	37.9	12.5	11.3	156

Based on the work presented in this report, the following conclusions can be drawn:

- The presented stress estimates from using indirect methods confirm, to a large extent, the stress state inferred from overcoring data alone.
- Re-calculation of overcoring data to fit a theoretical vertical stress ($\sigma_v = \rho gz$), gave somewhat lower horizontal stresses compared to overcoring data (a reduction of 1–5 MPa) but with stress orientations virtually unaffected.
- The maximum horizontal stress in borehole KFM01B reaches at least 35 MPa already at approximately 250 m depth.
- Higher stresses are likely at larger depths – this study suggests that stresses at 400 to 450 m depth reach 40 MPa. Core discing data from Level 2 indicate that the maximum horizontal stress may be even higher at these depths.
- No clear correlations could be found between rock types and measurement results, as all successful measurements were taken in similar rock types. However, measurements at Level 1 were located in much better rock in terms of fracture frequency and presence of open fractures. Hence, it is not surprising that the measured stresses were as high, or in some cases higher, at Level 1. The difference in stress orientation measured at Level 1 and Level 2 could not be correlated to the presence of e.g. geological structures.

- Examination of thin sections revealed that vertical, tangential fractures had developed close to the pilot hole wall. These fractures were interpreted as the initiation stage of spalling failure in the pilot hole wall. A higher fracture frequency was also found for certain circumferential orientations of the thin sections, which could be tentatively linked to the thin sections with the highest fracture frequency. The strong indications of spalling failure in the pilot hole wall can thus be a possible explanation to the observed premature debonding of strain gauges for several overcoring tests on Level 2.
- P-wave velocity measurements from borehole KFM01A support the notion of increased core damage potential below 500 m depth, but above this level and up to the ground surface, conditions are virtually constant. Stress orientations could not be reliably determined from P-wave data.

7 References

Amadei B, Stephansson O, 1997. Rock stress and its measurement. London: Chapman & Hall, 490 pp.

Berglund J, 2004. Additional data from detailed core logging of borehole KFM01B. Internal working material.

Berglund J, Petersson J, Wängnerud A, Danielsson P, 2004. Boremap mapping of core drilled borehole KFM01B. SKB P-04-114. Svensk Kärnbränslehantering AB.

Cai M, Kaiser P K, Tasaka Y, Maejima T, Morioka H, Minami M, 2004. Generalized crack initiation and crack damage stress thresholds of brittle rock masses near underground excavations. Int. J. Rock Mech. Min. Sci, 41, pp 833–847.

Carlsson B, Andersson Y, Lindfors U, Nordlund E, 1999. The failure process and the acoustic emission of brittle rock under compression. Proceedings of the 9th ISRM International Congress on Rock Mechanics (Paris, 1999), Vol. 2, pp 569–572. Rotterdam: A. A. Balkema.

Diederichs M S, 2003. Rock fracture and collapse under low confinement conditions. Rock Mech. Rock Engng, 36(5), pp 339–381.

Diederichs M S, Kaiser P K, Eberhardt E, 2004. Damage initiation and propagation in hard rock during tunneling and the influence of near-face stress rotation. Int. J. Rock Mech. Min. Sci, 41, pp 785–812.

Dzik E J, 2004. Personal communication.

Eloranta P, 2004. Drill hole KFM01A: Indirect tensile strength test (HUT). SKB P-04-171. Svensk Kärnbränslehantering AB.

Forssberg O, Staub I, 2004. RVS model KFM01B. SKB P-report P-04-XX (in preparation). Svensk Kärnbränslehantering AB.

Hakala M, 1999a. Numerical study on core damage and interpretation of in situ state of stress. Posiva report 99-25.

Hakala M, 1999b. Numerical study of the core disk fracturing and interpretation of the in situ state of stress. Proc. Ninth International Congress on Rock Mechanics (Paris, 1999), Vol. 2, pp 1149–1153. Rotterdam: A. A. Balkema.

Hakala M, 2000. Interpretation of the Hästholmen in situ state of stress based on core damage observations. Posiva report 2000-01.

Hakala M, 2004. Personal communication.

Hakala M, Hudson J A, Christiansson R, 2003. Quality control of overcoring stress measurement data. Int. J. Rock Mech. Min. Sci, 40, No 7–8, pp 1141–1159.

Jacobsson L, 2004. Drill hole KFM01A. Indirect tensile strength test. SKB P-04-170. Svensk Kärnbränslehantering AB.

Martin C D, Christiansson R, Söderhäll J, 2001. Rock stability considerations for siting and constructing a KBS-3 repository. SKB TR-report, TR-01-38.

Martin C D, Stimpson B, 1994. The effect of sample disturbance on laboratory properties of Lac du Bonnet granite. Canadian Geotechnical Journal, 31(5), pp 692–702.

Petersson J, Wängnerud A, 2003. Boremap mapping of telescopic drilled borehole KFM01A. SKB P-03-23. Svensk Kärnbränslehantering AB.

Rocscience, 2004. Dips. Version 5.1. Toronto: Rocscience, Inc.

Sjöberg J, 2004. Overcoring rock stress measurements in borehole KFM01B. SKB P-04-83. Svensk Kärnbränslehantering AB.

Sjöberg J, Klasson H, 2003. Stress measurements in deep boreholes using the Borre (SSPB) probe. Int. J. Rock Mech. Min. Sci, 40, No 7–8, pp 1205–1233.

Staub I, 2003. KFM01A: RVS model of fractures. Prediction of sections for stress measurements in KFM01B. SKB P-03-85. Svensk Kärnbränslehantering AB.

SKB, 2004a. Preliminary site description. Forsmark area – version 1.1. SKB R-04-15. Svensk Kärnbränslehantering AB.

SKB, 2004b. SICADA information obtained from SKB. Strength data for rock types at Forsmark.

SKB, 2004c. SICADA information obtained from SKB. Fracture frequency data from KFM01B & KFM01A.

Tunbridge L, Chryssanthakis P, 2003. Borehole: KFM01A. Determination of P-wave velocity, transverse borehole core. SKB P-03-38. Svensk Kärnbränslehantering AB.

Walker J R, Martin C D, Dzik E J, 1990. Technical Note: Confidence intervals for in situ stress measurements. Int. J. Rock Mech. Min. Sci. & Geomech. Abstr, 27, No 2, pp 139–141.

Appendix A

Computer program for calculation of confidence intervals

Theory and implementation

Since stress is a tensor with six independent components, calculation of average values and confidence intervals cannot be conducted using conventional statistical methods for scalar quantities. /Walker et al. 1990/ described a methodology for calculating confidence intervals for in situ stress measurements. The methodology is based on the Monte-Carlo technique and the assumption that a normal probability distribution function applies to in situ stresses. The real probability distribution function is currently unknown; however, should such information become available, the methodology can be easily adopted for any distribution function.

The original computer program for this methodology was developed for Atomic Energy for Canada Limited (AECL) for use in mainframe computers. The program was called COSTUM and was also classified as proprietary by AECL. For these reasons, it was decided to rewrite the code in a more modern format, making use of existing applications as far as possible. The code was developed according to the methodology described by /Walker et al. 1990/ and with additional clarifications provided by /Dzik, 2004/.

The computer program was developed as a Microsoft Excel application using VBA. Calculation of confidence intervals is performed with the Excel application and presented in summary tables for the stress magnitudes. In the present version, 20,000 Monte-Carlo simulations are performed, but this may be changed in future versions (if the need arises). Presentation of confidence intervals for principal stress orientations is conducted using the Dips computer package /Rocscience, 2004/ with input files generated from the Excel application.

Manual for operation

Installation

The code was developed and tested in Microsoft Windows 2000, using Microsoft Excel 2000. It should run also in Windows XP/Office XP and future versions.

To install the code, simply copy the file “Confidence_stress.xls” to any folder of your choice. No additional files are required. However, Microsoft Excel must be configured so that macros can be run, see Figure A1.

For plotting of confidence intervals for stress orientations, the Dips computer program is required. The program can be purchased from Rocscience, Inc. (URL: www.rocscience.com). For installation of this program, please refer to the documentation provided with the program.

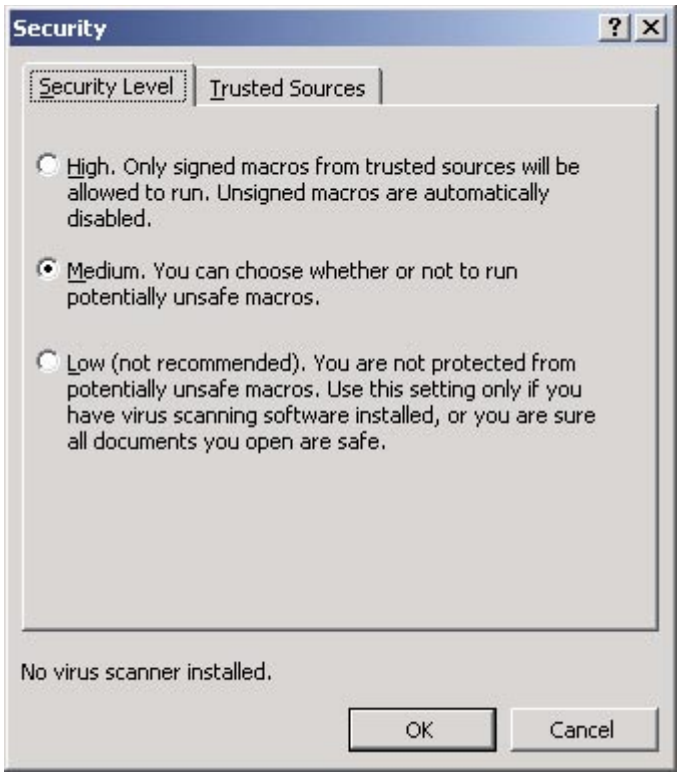

Figure A1. *Required security settings for Microsoft Excel.*

Operation

Start the program by double-clicking the file "Confidence_stress.xls". Excel first performs a check that macros are allowed to run. Click "Enable Macros" to ensure proper operation of the application. The program then requests the user to save the file under a new name, see Figure A2.

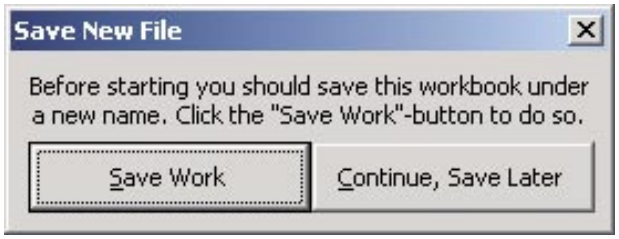

Figure A2. *Save file under new name.*

Next, the screen in Figure A3 is shown. To fill in data from stress measurements, type these directly in the yellow-marked fields. The required input is magnitude, dip, and bearing for each of the three principal stresses (σ_1, σ_2, σ_3). Additionally, the depth at which measurements were taken may be filled in for later plotting of stresses vs. depth. Note that at least two measurements must be input for statistical calculation. In the current version, a maximum of 10 stress measurements can be input.

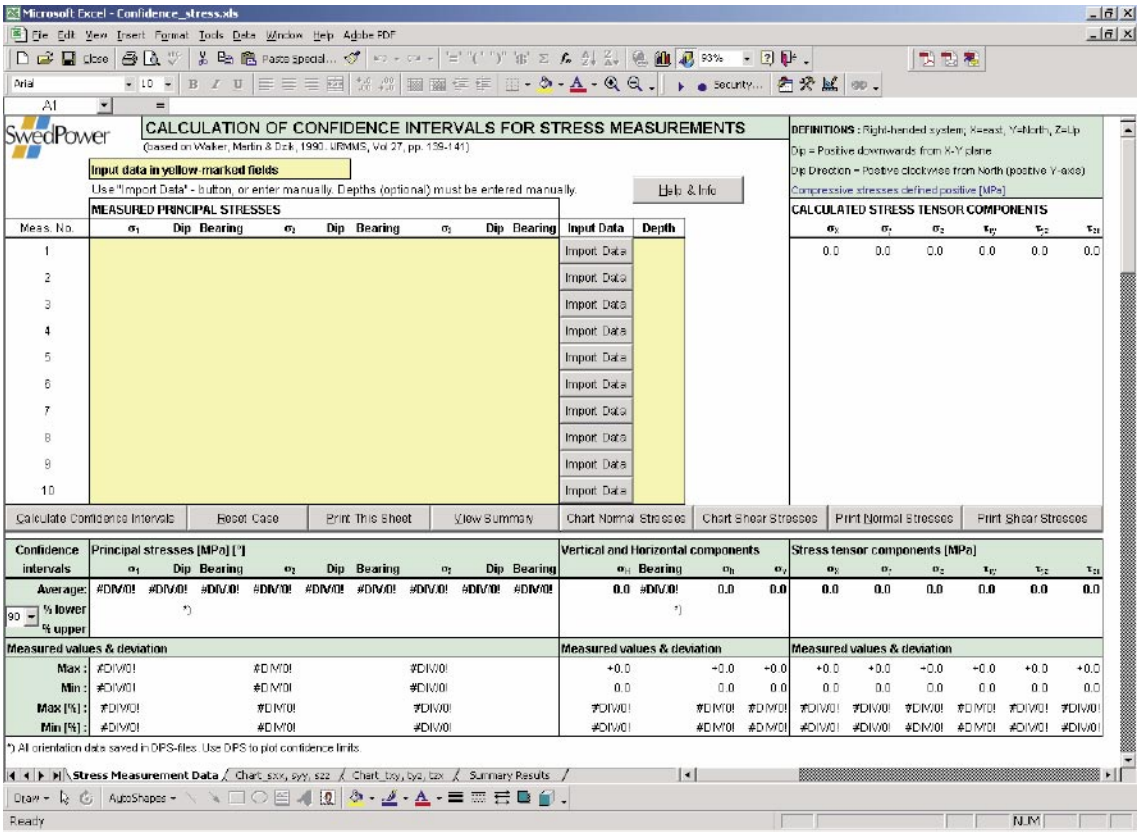

Figure A3. *Main worksheet screen.*

As an alternative to manual input, data can imported from results-files (*.res) generated by the stress calculation program for the Borre probe (see also SKB MD 181.001, SKB internal controlling document). These files are in comma-separated ASCII-format with the format and contents described in Figure A4.

```
Borehole_dip,Borehole_bearing,Compass_value,E_modulus,Poisson_ratio,
strain_e1,strain_e2,_strain_e3,strain_e4,strain_e5,strain_e6,strain_e7
,strain_e8,strain_e9,sigma_1,sigma_1_dip,sigma_1_bearing,sigma_2,
sigma_2_dip,sigma_2_bearing,sigma_3,sigma_3_dip, sigma_3_bearing,
sigma_H,sigma_H_bearing,sigma_h,sigma_h_bearing,sigma_v,error_value,↵
"Start-time", "Stop-time"

72,269.7,120,67.8,.35,450,1236,1238,202,873,475,308,225,-342,56,35.4,
222,36.5,50,74.3,15.7,16.2,323.9,49.1,49.1,17.7,139.1,41.4,47896
"Start=10:16:30","Stop=10:35:00"
```

Figure A4. *Format of *.res-files (top) and example of *.res-file (bottom). Note that the values are input as one long row of comma-separated data, with the exception of the last two items ("Start-time" and "Stop-time").*

Once all data are input, press the button "Calculate Confidence Intervals", see Figure A5. Calculation times differ depending on computer configuration and number of stress measurements, but normally vary between 5 and 30 minutes. During calculation, a message box is displayed, and the program locked for input and/or changes.

After completed calculation, a message is shown. The user is then asked to provide file names for Dips-files for saving calculated confidence data for the stress orientations (Figure A6). These are saved in five separate files, one for each principal stress (σ_1, σ_2, σ_3), one for the major horizontal stress (σ_H) and for the orientation of the average principal stresses for this particular set of measurements.

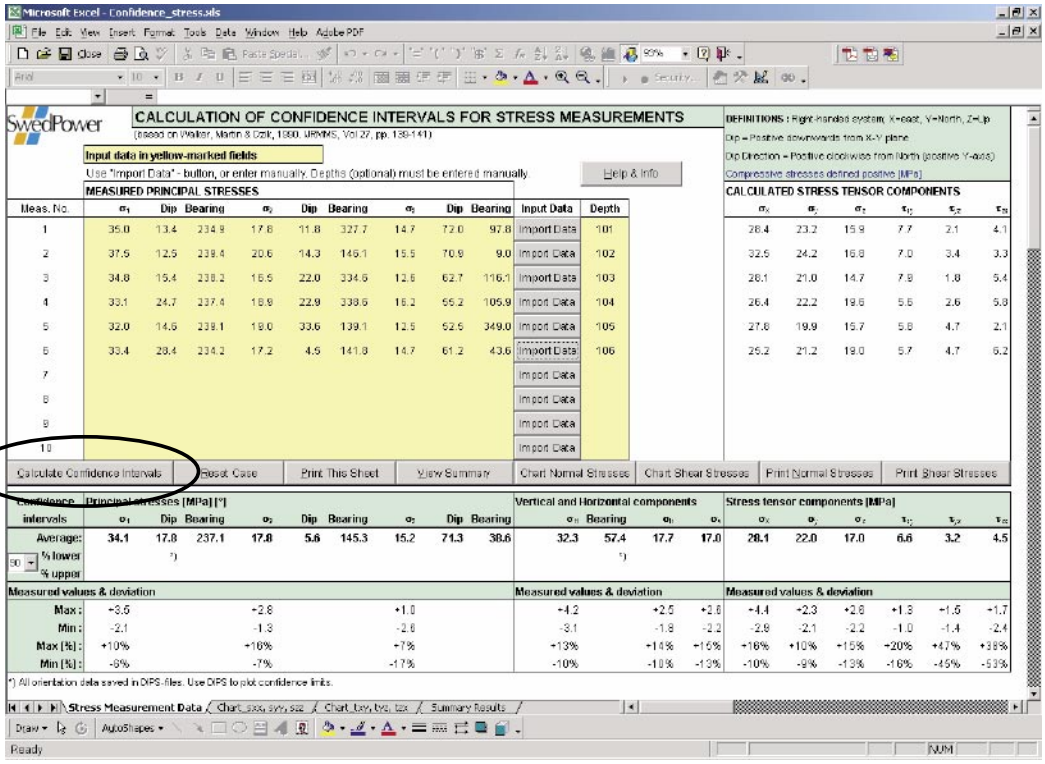

Figure A5. *Data from six stress measurements input; ready for calculation start.*

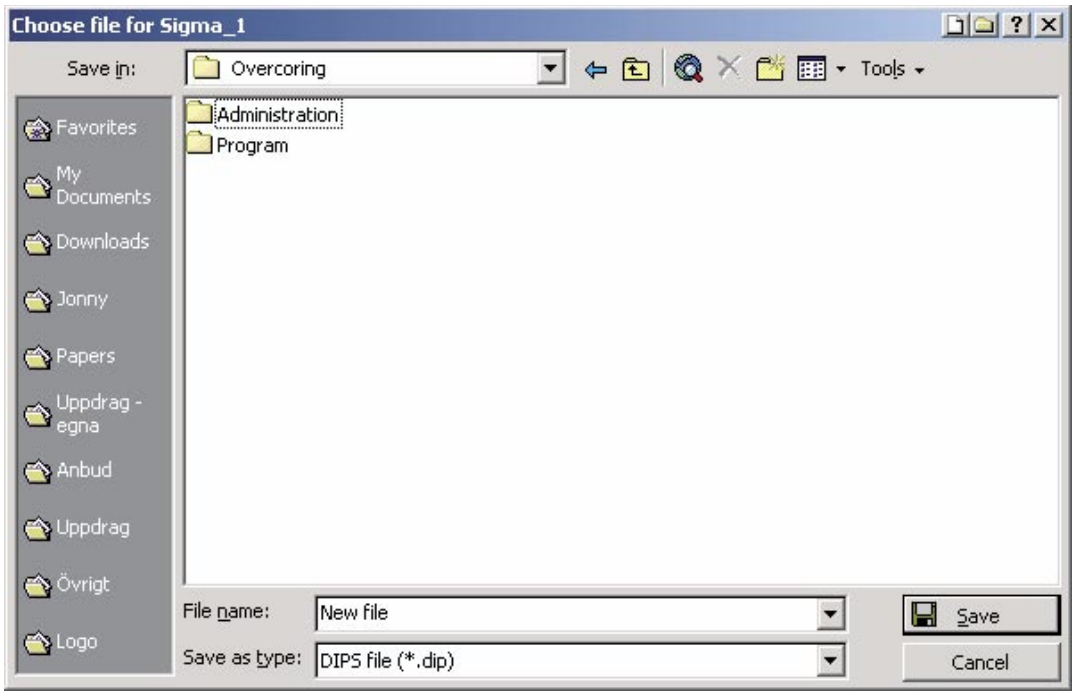

Figure A6. *Saving Dips-files with stress orientation data.*

Presentation of confidence intervals – magnitudes and average orientations

The calculated confidence intervals in terms of magnitudes, along with the average principal stress orientations, are presented directly on the input worksheet, see Figure A7. By clicking the drop-down list, the user can choose to display 95%-, 90%-, or 80%-confidence limits. A full summary of the confidence intervals for (i) each stress tensor component, (ii) vertical and horizontal stresses, and (iii) principal stresses, can be viewed by clicking the "View Summary"-button. An example is shown in Figure A8.

The user may also plot normal and/or shear stress versus measurement depth, for additional interpretation and evaluation of the results using the buttons on the input worksheet ("Stress Measurement Data"). To conduct calculation for a new set of measurements, reset the existing case by clicking the "Reset Case"-button.

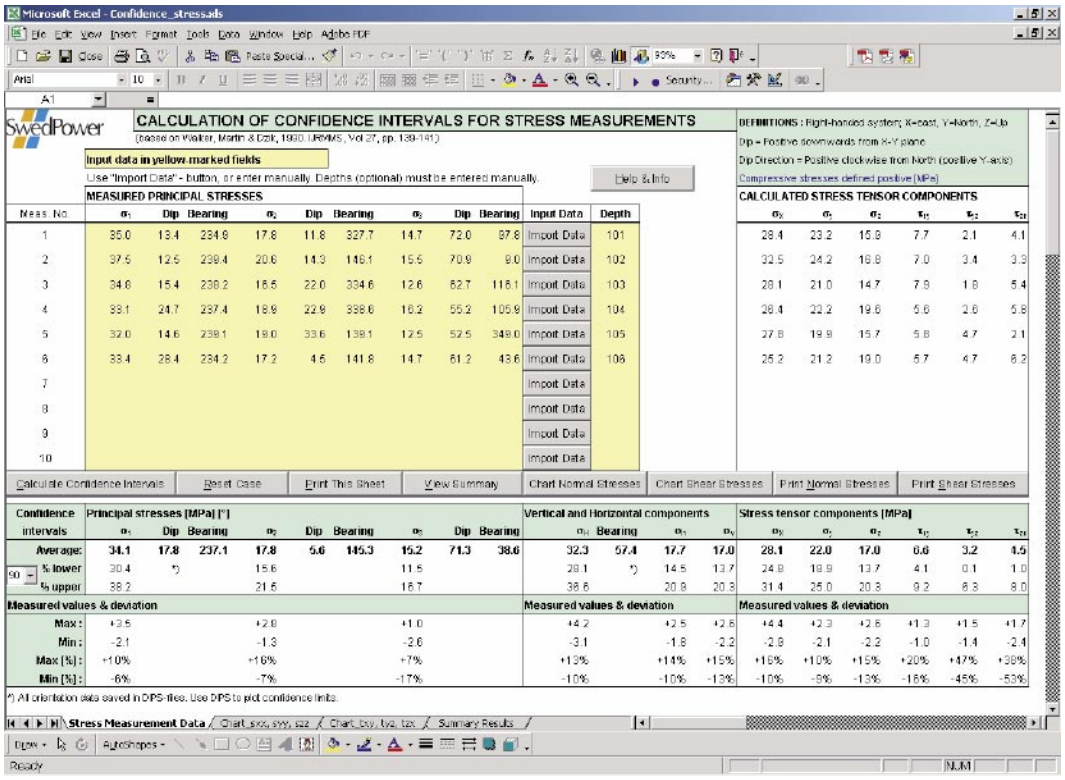

Figure A7. *Calculated confidence intervals and input data.*

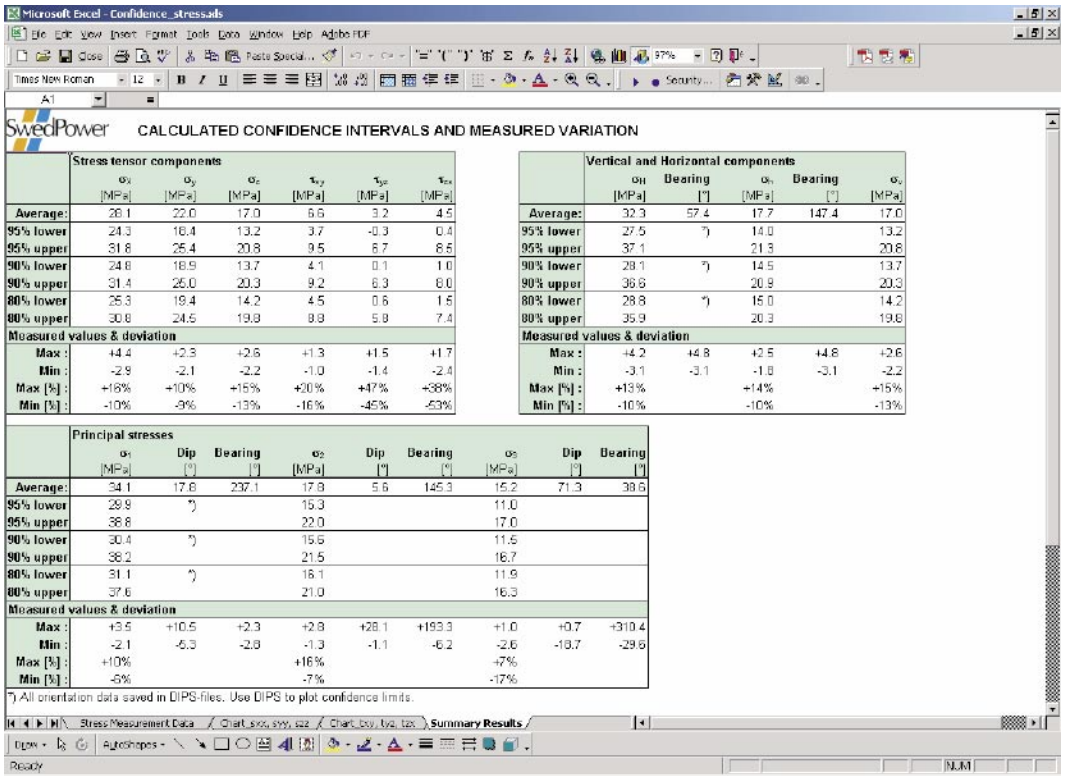

Figure A8. *Summary of calculated confidence intervals.*

Presentation of confidence intervals – principal stress orientations

The confidence intervals for the stress orientations are plotted using Dips. To open a file, double-click on it, or open the file from within Dips. An example of an opened file is shown in Figure A9. To view a contour plot, select “View”–“Contour Plot” from the menu, or click the corresponding icon on the toolbar (Figure A9).

To display a single contour for a chosen confidence limit, first select “Setup”–“Stereonet Options” and choose Distribution: “Schmidt”, as shown in Figure A10. Then, select “Setup”–“Contour Options” from the menu, or right-click on the contour plot and select “Contour Options”. On the displayed menu, select Format: “Custom”, Mode: “Lines”, and Number: “2”, see Figure A11. Click “Apply” and “OK” to apply the new settings to the contour plot. These settings can also be saved as default options by choosing “Setup”–“Auto Options”–“Save Current Options” from the menu and specifying an identifying name for the setup option.

To plot confidence intervals correctly, select “Setup”–“Contour Options” again and set Contour Range: “Custom Range” (Figure A11). For plotting 90%-confidence intervals, input “5” as both minimum- and maximum contour range. An example of the resulting contour plot of the confidence interval is shown in Figure A12. To plot other confidence limits, simply change the minimum- and maximum contour range (“2.5” for 95%-limits, “10” for 80%-limits, etc). For certain data sets (with large scatter), the 80%- or 90%-limits may not be possible to plot. This is normal as it simply means that a larger confidence interval (e.g. 95% or higher) is needed to encompass the highly scattered data. The above procedure is then repeated for all other stress components.

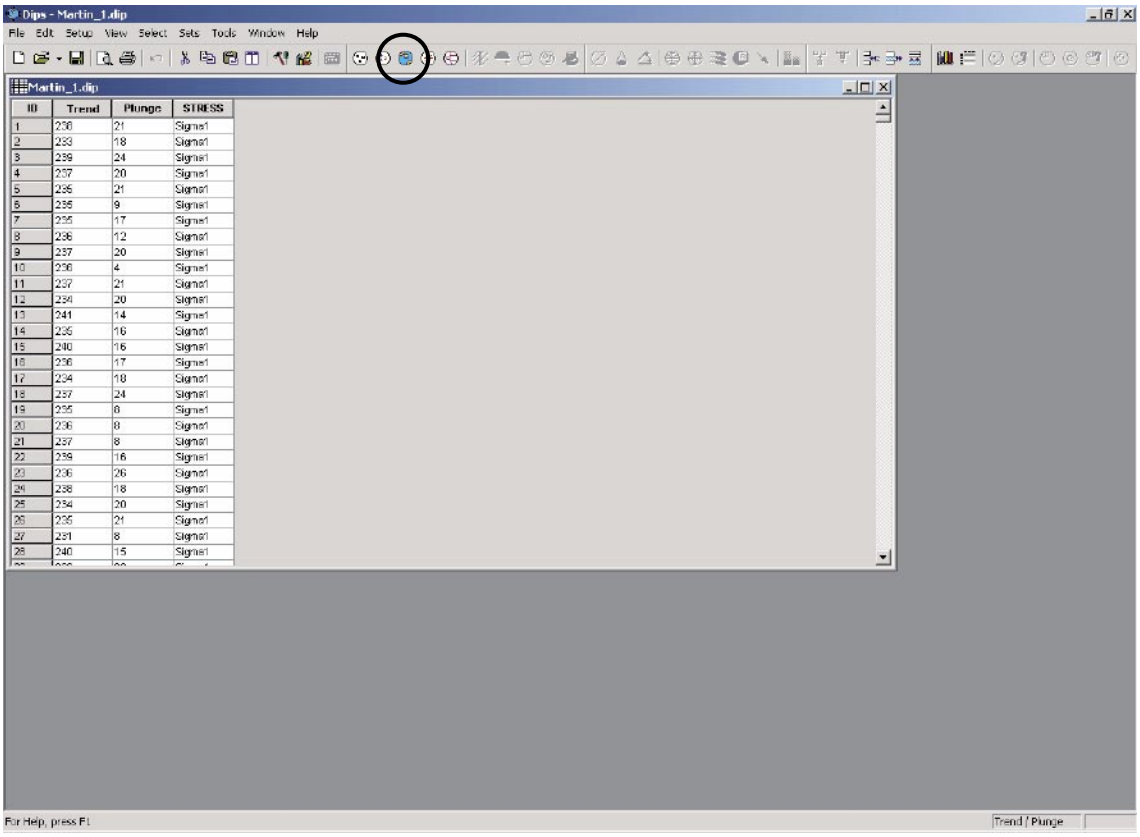

Figure A9. *Dips-file opened in the Dips-program.*

For plotting the average principal stress orientations, open the corresponding Dips-file and then choose “View”–“Pole Plot” from the menu. Right-click on the pole plot and choose “Symbolic Pole Plot”. Choose Plot Style: “Symbolic Pole Plot” and choose “Stress” from the drop-down list, see Figure A13. An example of the resulting pole plot, displaying both the principal stress orientations for each measurement as well as the average principal stress orientations, is shown in Figure A14.

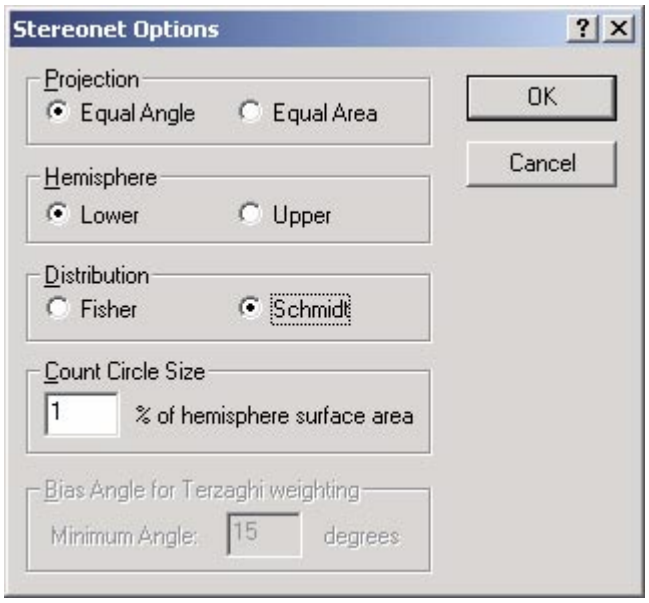

Figure A10. *Setting Stereonet Options in Dips.*

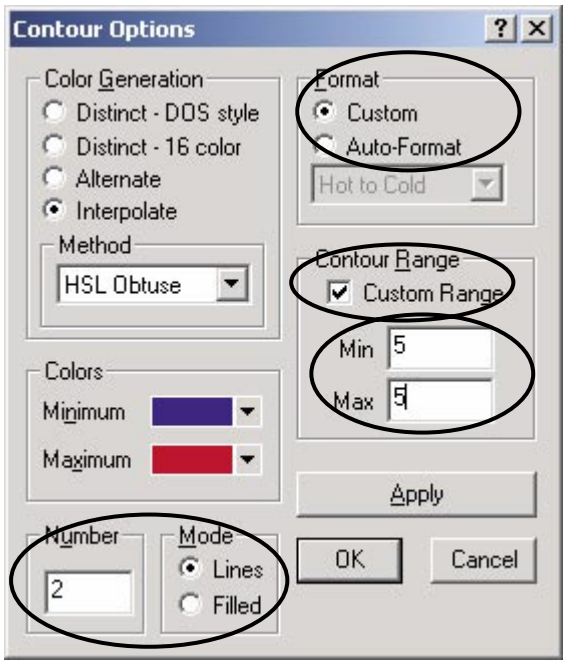

Figure A11. *Setting Contour Options in Dips.*

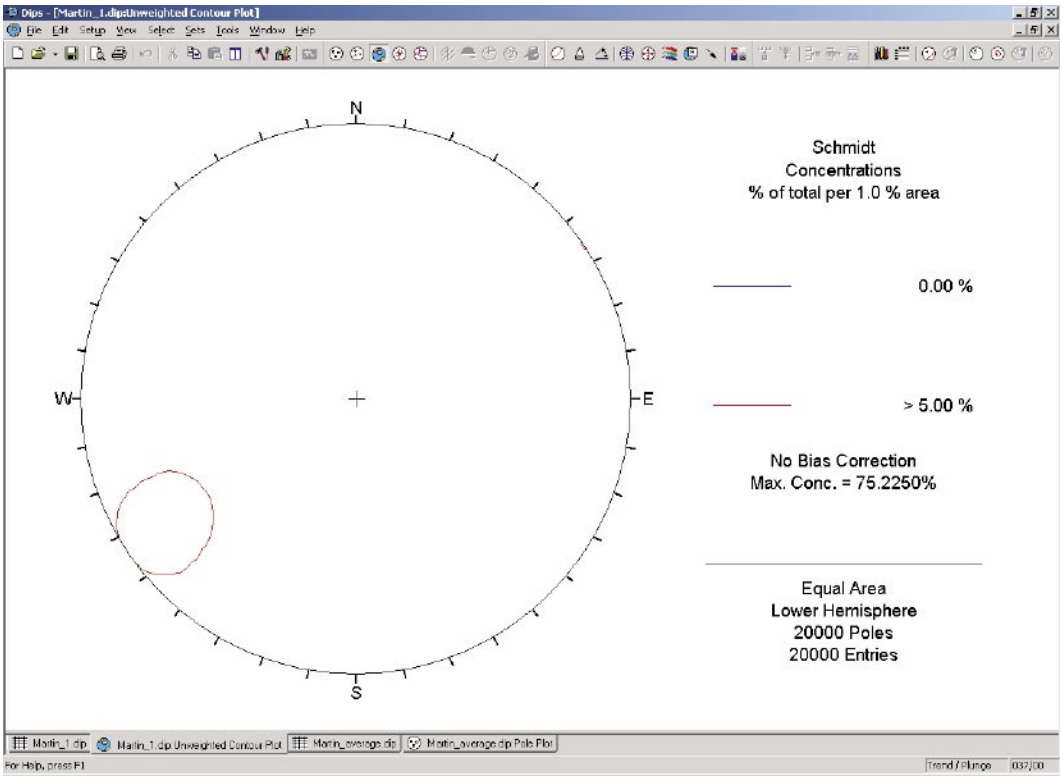

Figure A12. *Plotting of confidence limits for a chosen stress component.*

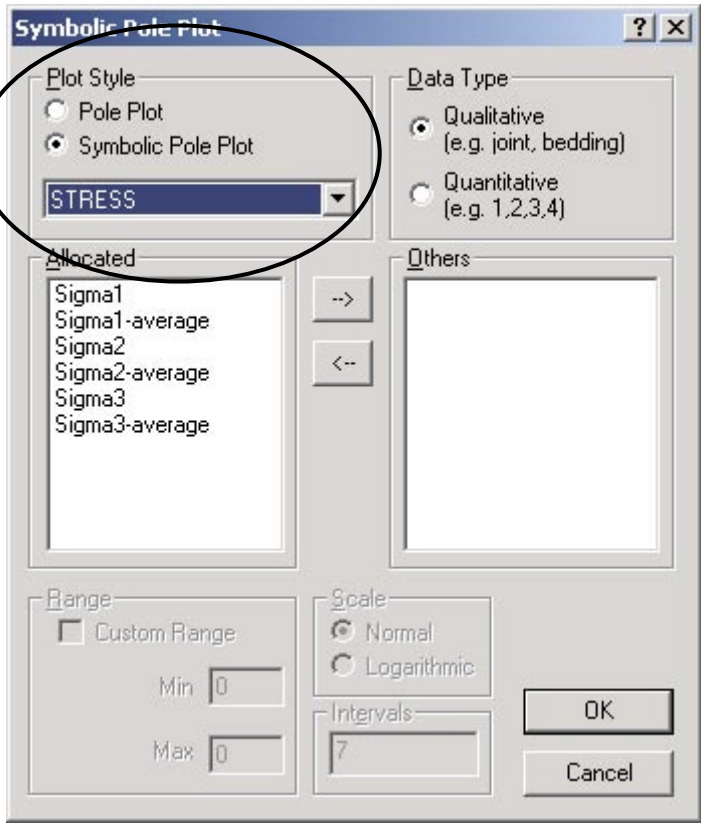

Figure A13. *Setting Symbolic Plot options in Dips.*

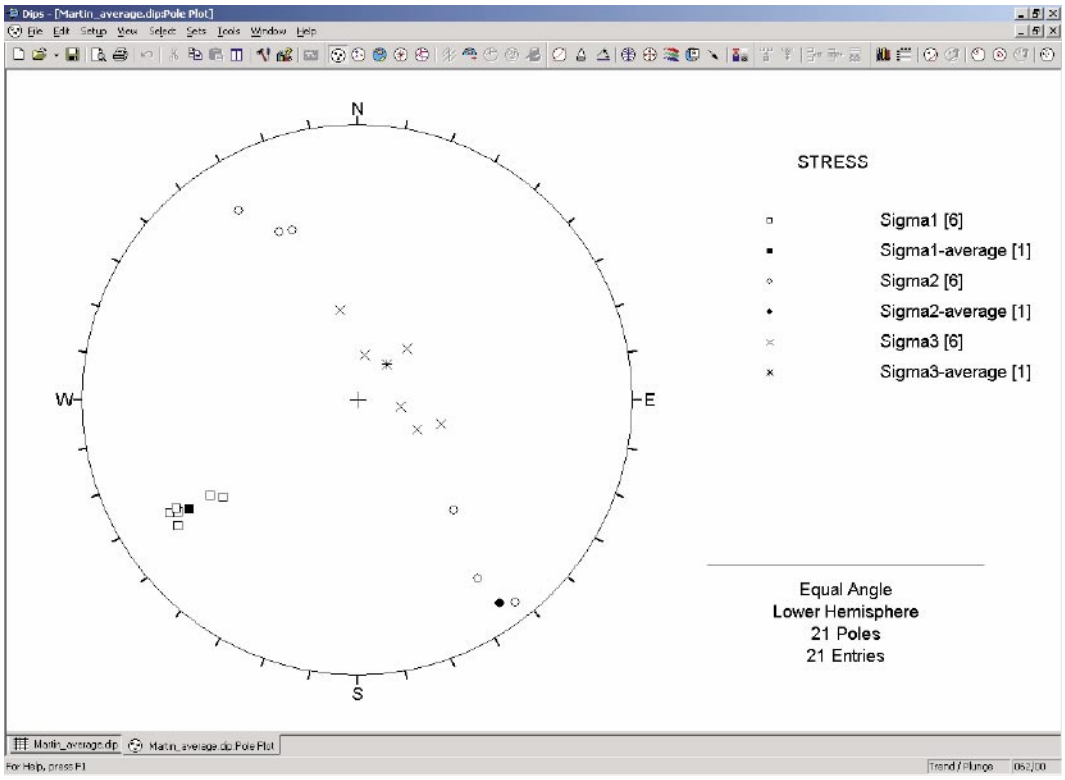

Figure A14. *Plotting of principal stress orientations and average principal stress orientations.*

Contact person

For additional help with the operation of the program, please contact the author at the following coordinates:

Jonny Sjöberg
SwedPower AB
SE-971 77 Luleå, SWEDEN
Phone: +46-920-77 353
Fax: +46-920-77 369
Email: jonny.sjoberg@swedpower.com

Appendix B

Results from mapping of thin sections

Table B1. Summary of horizontal thin sections.

Sample	H1	H2	H3	H4	H5	H6
Total amount of cracks	307	324	274	170	215	159
Vertical	49	26	28	49	16	23
Horizontal	18	44	38	33	50	27
/ (10°–80°)	84	133	159	31	87	75
\ (280°–350°)	157	121	49	57	62	34
Longer than 1 mm, Number/Mean (mm)	19/1.3	21/1.4	14/1.3	15/1.6	17/1.3	7/1.3
Between 0.5 mm–1 mm, Total/Mean (mm)	32/0.7	62/0.7	38/0.7	50/0.7	47/0.7	27/0.7
Shorter 0.5 mm, Number	256	241	222	105	151	125

Table B2. Sample H1.

Line	1	2	3	4	5	6
Total amount of cracks	64	88	51	26	54	24
Vertical	11	12	8	6	9	3
Horizontal	4	7	3	0	3	1
/ (10°–80°)	26	16	16	6	18	2
\ (280°–350°)	24	53	24	14	24	18
Longer 1 mm, Number/Total Length (mm)	1/10	10/117	2/21	1/10	4/42	1/9
Between 0.5 mm–1 mm, Number/Total Length (mm)	4/21	11/62	11/61	0/0	6/36	0/0
Shorter 0.5 mm, Number/Total Length (mm)	59	67	38	25	44	23

Table B3. Sample H2.

Line	1	2	3	4	5	6
Total amount of cracks	43	97	89	31	56	9
Vertical	4	10	4	5	3	0
Horizontal	12	8	14	3	5	2
/ (10°–80°)	11	40	39	12	27	5
\ (280°–350°)	16	39	32	11	21	2
Longer 1 mm, Number/Total Length (mm)	3/30	8/117	5/55	1/16	4/41	0/0
Between 0.5 mm–1 mm, Number/Total Length (mm)	7/41	24/148	16/94	2/12	11/72	2/10
Shorter 0.5 mm, Number/Total Length (mm)	33	65	68	28	41	7

Table B4. Sample H3.

Line	1	2	3	4	5	6
Total amount of cracks	36	78	73	34	27	27
Vertical	0	4	8	2	8	6
Horizontal	9	6	12	4	6	2
/ (10°–80°)	21	51	44	18	9	16
\ (280°–350°)	6	17	9	10	4	3
Longer 1 mm, Number/Total Length (mm)	2/21	4/45	7/77	0/0	1/19	0/0
Between 0.5 mm–1 mm, Number/Total Length (mm)	2/12	13/75	13/80	3/15	5/26	2/11
Shorter 0.5 mm, Number/Total Length (mm)	32	61	53	31	21	25

Table B5. Sample H4.

Line	1	2	3	4	5	6
Total amount of cracks	29	45	28	26	19	23
Vertical	4	12	5	6	11	11
Horizontal	5	14	5	5	2	2
/ (10°–80°)	7	8	8	4	3	1
\ (280°–350°)	13	11	10	11	3	9
Longer 1 mm, Number/Total Length (mm)	1/35	6/65	2/25	2/26	0/0	4/62
Between 0.5 mm–1 mm, Number/Total Length (mm)	8/45	13/75	8/48	11/65	3/19	7/37
Shorter 0.5 mm, Number/Total Length (mm)	20	26	18	13	16	12

Table B6. Sample H5.

Line	1	2	3	4	5	6
Total amount of cracks	44	55	43	28	18	27
Vertical	2	1	6	3	4	0
Horizontal	15	18	5	7	2	3
/ (10°–80°)	13	21	21	9	5	19
\ (280°–350°)	14	15	11	9	7	5
Longer 1 mm, Number/Total Length (mm)	2/18	5/52	3/44	4/41	0/0	3/42
Between 0.5 mm–1 mm, Number/Total Length (mm)	11/69	9/54	6/35	3/20	11/66	7/45
Shorter 0.5 mm, Number/Total Length (mm)	31	41	34	21	7	17

Table B7. Sample H6.

Line	1	2	3	4	5	6
Total amount of cracks	30	47	28	10	22	21
Vertical	1	7	4	0	3	7
Horizontal	11	10	3	0	0	3
/ (10°–80°)	9	21	16	6	14	9
\ (280°–350°)	9	9	5	4	5	2
Longer 1 mm, Number/Total Length (mm)	0/0	3/31	0/0	2/30	1/9	1/9
Between 0.5 mm–1 mm, Number/Total Length (mm)	7/40	3/20	7/41	2/12	5/34	3/18
Shorter 0.5 mm, Number/Total Length (mm)	23	41	21	6	16	17

Table B8. Summary of vertical thin sections.

Sample	V1	V2	V3	V4	V5	V6
Total amount of cracks	249	449	149	470	204	206
Vertical	80	45	43	98	61	37
Horizontal	47	74	24	44	60	41
/ (10°–80°)	35	160	46	167	34	60
\ (280°–350°)	86	170	36	161	49	68
Longer than 1 mm, Number/Mean (mm)	56/2.0	12/2.0	14/1.3	26/1.8	35/1.6	22/1.8
Between 0.5 mm–1 mm, Total/Mean (mm)	68/0.7	66/0.7	41/0.7	88/0.7	64/0.7	52/0.7
Shorter 0.5 mm, Number	124	371	94	356	105	132

Table B9. Sample V1.

Line	1	2	3	4	5	6	7	8	9*
Total amount of cracks	38	51	46	9	23	22	24	35	–
Vertical	9	16	19	1	4	12	9	10	–
Horizontal	10	19	7	1	2	2	0	6	–
/ (10°–80°)	4	3	10	1	7	3	2	5	–
\ (280°–350°)	15	13	10	6	10	5	13	14	–
Longer 1 mm, Number/Total Length (mm)	7/120	8/116	17/295	3/41	12/142	4/59	2/34	3/45	–
Between 0.5 mm–1 mm, Number/Total Length (mm)	14/77	11/60	14/84	1/6	3/17	10/57	7/47	8/45	–
Shorter 0.5 mm, Number/Total Length (mm)	17	32	15	5	8	8	15	24	–

***** The line is outside the rock slice

Table B10. Sample V2.

Line	1	2	3	4	5	6	7	8	9
Total amount of cracks	60	73	66	17	55	48	63	34	33
Vertical	4	10	2	2	5	6	8	3	5
Horizontal	18	11	8	3	9	4	14	1	6
/ (10°–80°)	24	22	30	5	9	15	26	13	16
\ (280°–350°)	14	30	26	7	32	23	15	17	6
Longer 1 mm, Number/Total Length (mm)	2/19	2/103	0/0	0/0	0/0	1/11	1/13	5/53	1/12
Between 0.5 mm–1 mm, Number/Total Length (mm)	6/38	13/83	12/72	3/18	6/33	2/11	10/59	10/59	4/23
Shorter 0.5 mm, Number/ Total Length (mm)	52	58	54	14	49	45	52	19	28

Table B11. Sample V3.

Line	1	2	3	4*	5	6	7	8	9*
Total amount of cracks	12	25	25	–	14	20	31	22	–
Vertical	2	5	8	–	4	3	11	10	–
Horizontal	4	8	5	–		3	3	1	–
/ (10°–80°)	5	7	7	–	3	9	8	7	–
\ (280°–350°)	1	5	5	–	7	5	9	4	–
Longer 1 mm, Number/Total Length (mm)	2/21	5/55	0/0	–	2/31	0/0	3/34	2/21	–
Between 0.5 mm–1 mm, Number/Total Length (mm)	6/34	5/27	8/46	–	2/12	6/32	9/52	5/30	–
Shorter 0.5 mm, Number/Total Length (mm)	4	15	17	–	10	14	19	15	–

***** The line is outside the rock slice

Table B12. Sample V4.

Line	1	2	3	4	5	6	7	8	9
Total amount of cracks	49	68	50	36	57	77	48	57	28
Vertical	8	15	10	7	12	20	15	8	3
Horizontal	10	5	6	3	5	5	4	4	2
/ (10°–80°)	10	31	20	13	23	27	12	19	12
\ (280°–350°)	21	17	14	13	17	25	17	26	11
Longer 1 mm, Number/Total Length (mm)	3/46	7/119	2/74	3/35	4/51	2/19	2/24	3/36	0/0
Between 0.5 mm–1 mm, Number/Total Length (mm)	4/20	16/92	7/38	7/39	10/66	12/70	12/70	13/75	7/41
Shorter 0.5 mm, Number/Total Length (mm)	42	45	41	26	43	63	34	41	21

Table B13. Sample V5.

Line	1	2	3	4	5	6	7	8	9
Total amount of cracks	30	36	40	7	18	26	6	24	17
Vertical	3	8	10	4	7	12	3	7	7
Horizontal	11	12	19	1	3	4	1	8	1
/ (10°–80°)	5	3	6	1	3	4	1	5	6
\ (280°–350°)	11	13	5	1	5	6	1	4	3
Longer 1 mm, Number/Total Length (mm)	9/102	4/54	12/198	2/23	3/54	2/34	0/0	2/20	1/9
Between 0.5 mm–1 mm, Number/Total Length (mm)	10/56	10/62	11/71	5/34	5/27	9/52	2/15	5/27	7/39
Shorter 0.5 mm, Number/ Total Length (mm)	11	22	17	0	10	15	4	17	9

Table B14. Sample V6.

Line	1	2	3	4*	5	6	7	8	9*
Total amount of cracks	28	36	39	–	29	25	19	30	–
Vertical	3	3	1	–	6	5	6	13	–
Horizontal	9	5	8	–	6	7	5	1	–
/ (10°–80°)	6	14	12	–	10	7	4	7	–
\ (280°–350°)	10	14	18	–	7	6	4	9	–
Longer 1 mm, Number/Total Length (mm)	1/70	9/103	9/147	–	1/11	0/0	1/10	1/10	–
Between 0.5 mm–1 mm, Number/Total Length (mm)	6/37	11/61	9/55	–	5/28	4/25	9/55	8/45	–
Shorter 0.5 mm, Number/ Total Length (mm)	21	16	21	–	23	21	9	21	–

***** The line is outside the rock slice

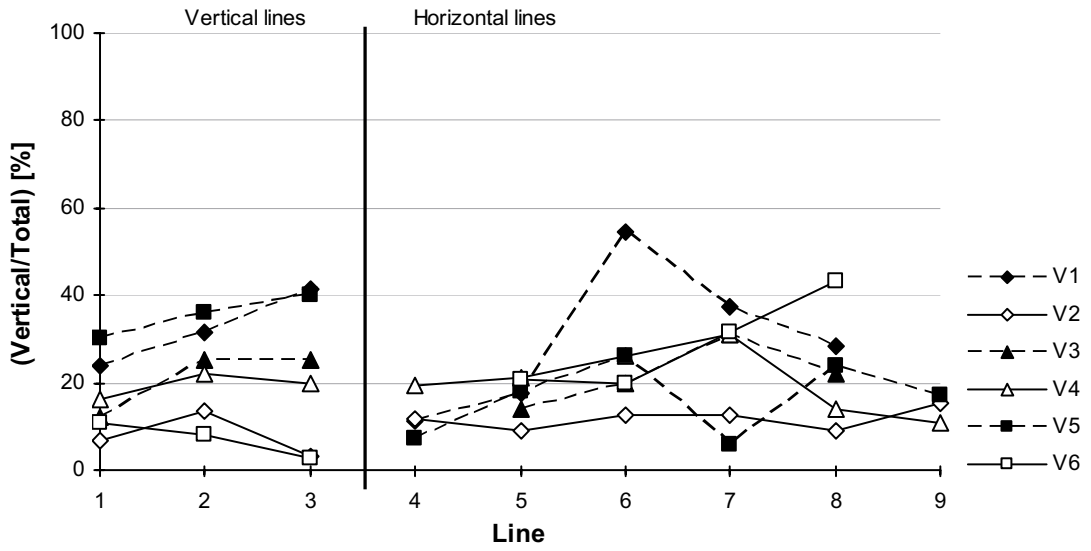

Figure B1. *Ratio between vertical microcracks and the total number of mapped microcracks on the vertical thin sections. Lines on the vertical thin sections are labelled horizontal and vertical since they are oriented in that way (cf Figure 4-7a).*

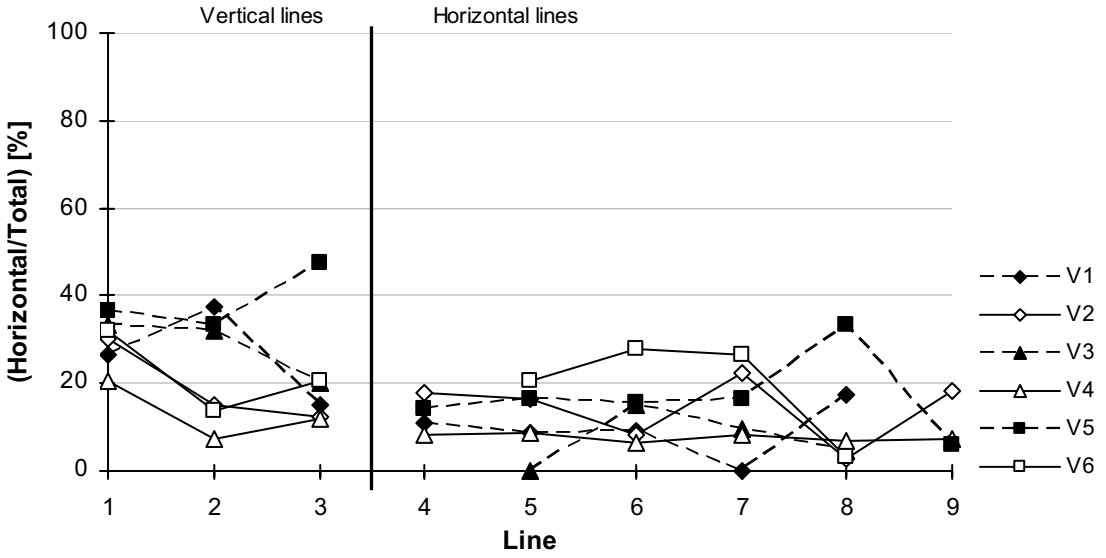

Figure B2. *Ratio between horizontal microcracks and the total number of mapped microcracks on the vertical thin sections. Lines on the vertical thin sections are labelled horizontal and vertical since they are oriented in that way (cf Figure 4-7a).*

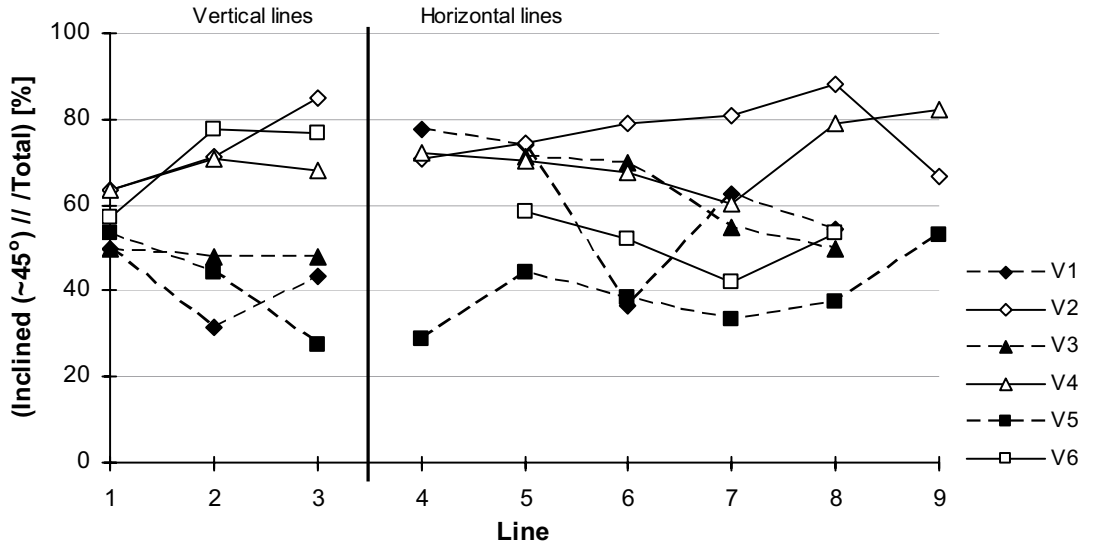

Figure B3. *Ratio between inclined microcracks and the total number of mapped microcracks on the vertical thin sections. Lines on the vertical thin sections are labelled horizontal and vertical since they are oriented in that way (cf Figure 4-7a).*

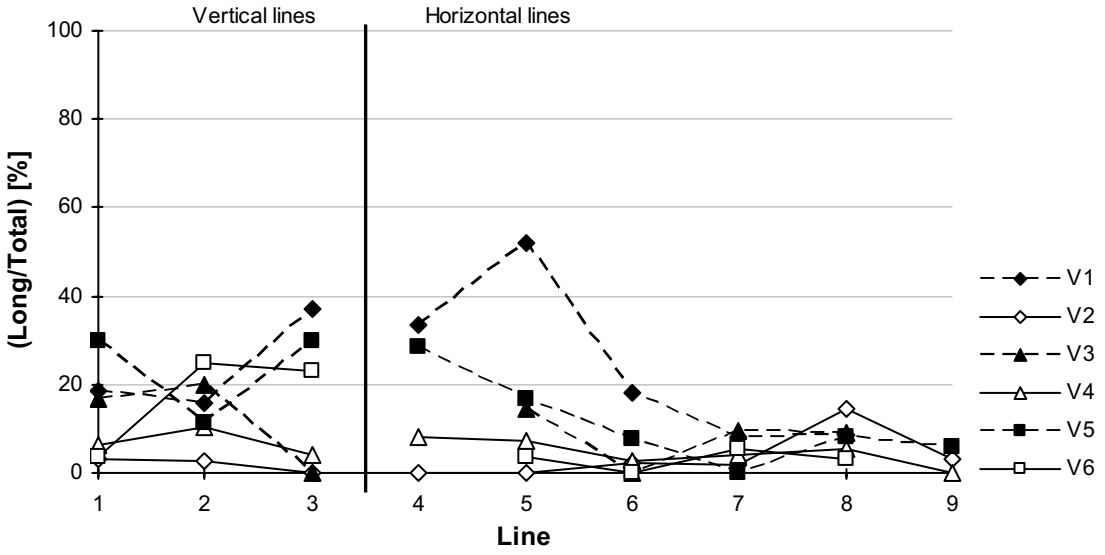

Figure B4. *Ratio between long microcracks and the total number of mapped microcracks on the vertical thin sections. Lines on the vertical thin sections are labelled horizontal and vertical since they are oriented in that way (cf Figure 4-7a).*

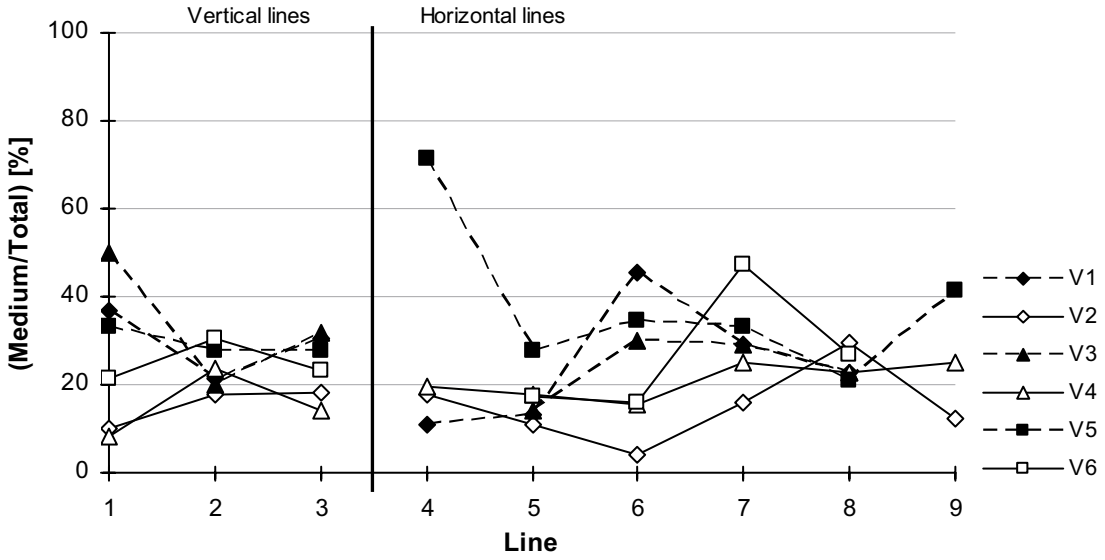

Figure B5. *Ratio between medium long microcracks and the total number of mapped microcracks on the vertical thin sections. Lines on the vertical thin sections are labelled horizontal and vertical since they are oriented in that way (cf Figure 4-7a).*

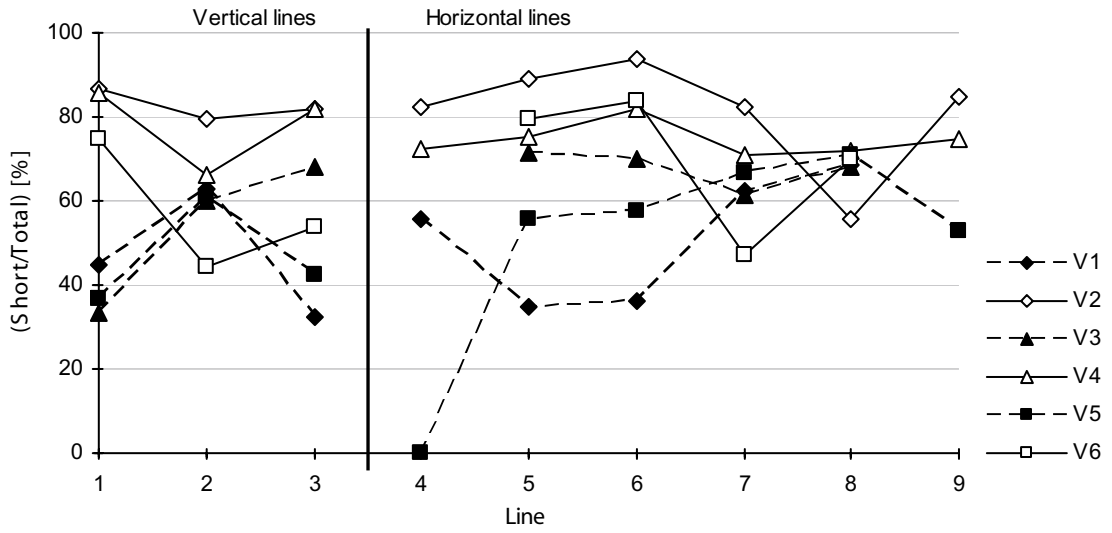

Figure B6. *Ratio between short microcracks and the total number of mapped microcracks on the vertical thin sections. Lines on the vertical thin sections are labelled horizontal and vertical since they are oriented in that way (cf Figure 4-7a).*

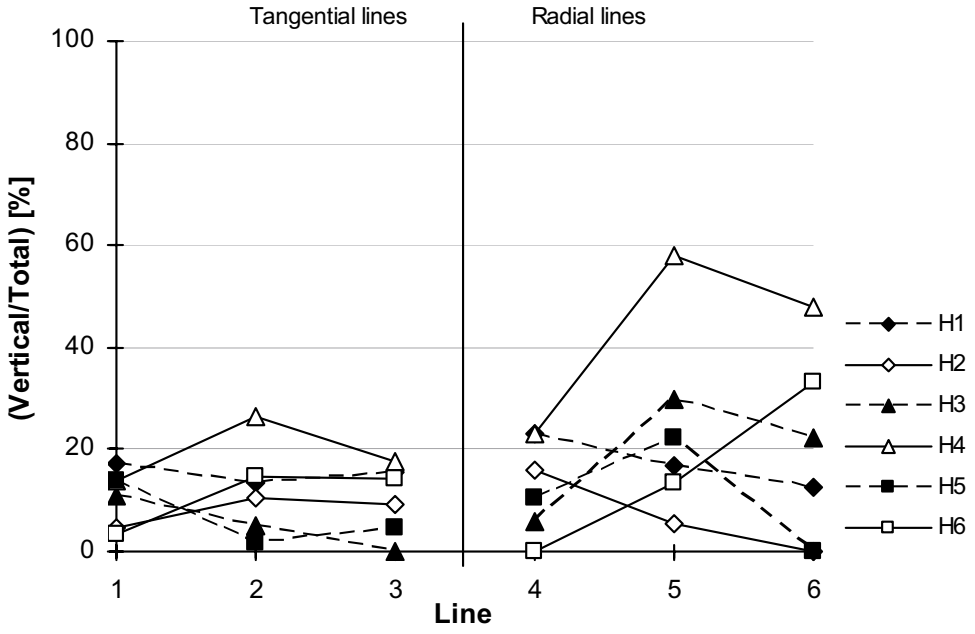

Figure B7. *Ratio between tangential microcracks and the total number of mapped microcracks on the horizontal thin sections. Lines on the horizontal thin sections are labelled tangential and radial (cf Figure 4-7b).*

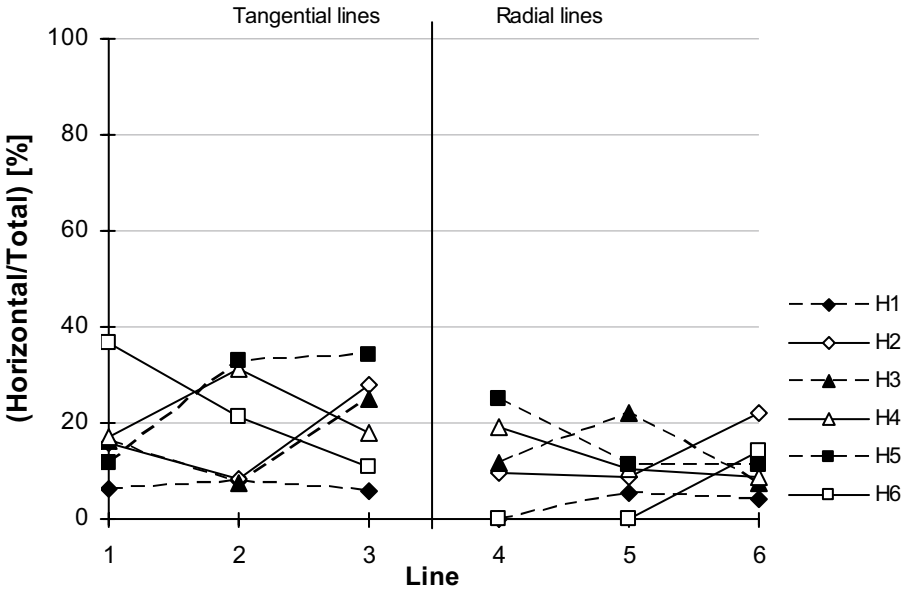

Figure B8. *Ratio between radial microcracks and the total number of mapped microcracks on the horizontal thin sections. Lines on the horizontal thin sections are labelled tangential and radial (cf Figure 4-7b).*

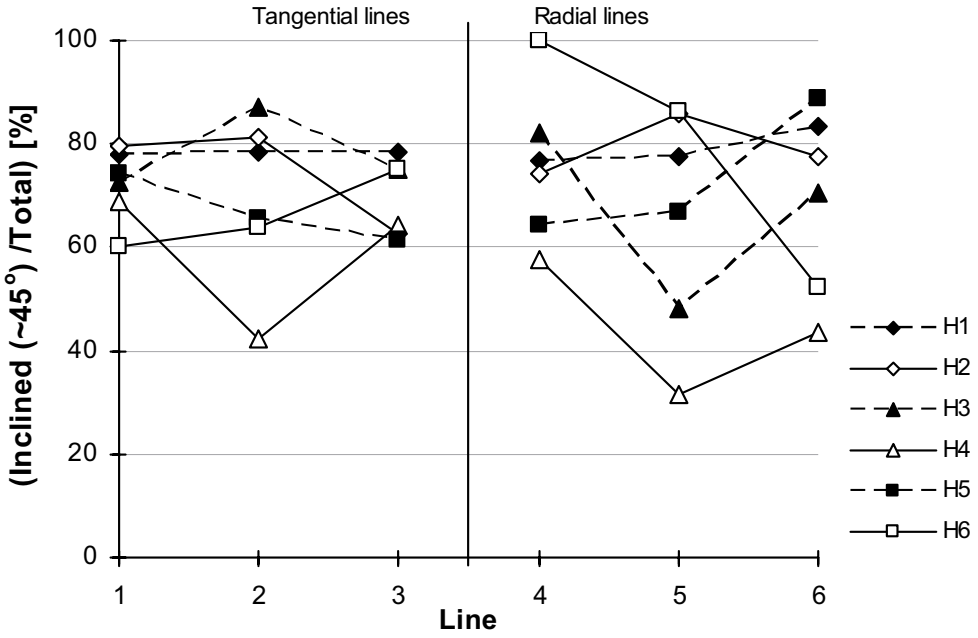

Figure B9. *Ratio between inclined microcracks and the total number of mapped microcracks on the horizontal thin sections. Lines on the horizontal thin sections are labelled tangential and radial (cf Figure 4-7b).*

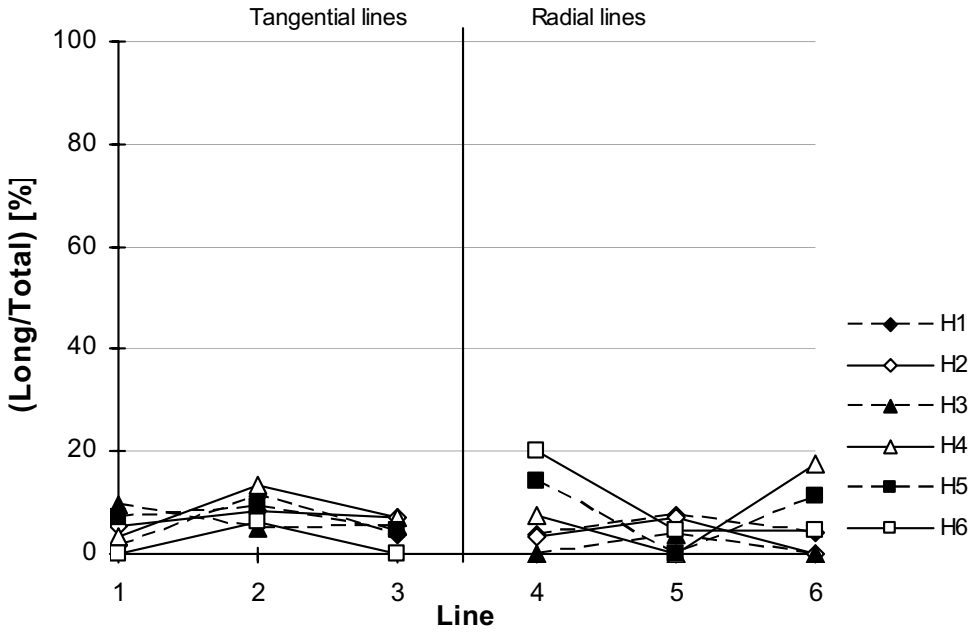

Figure B10. *Ratio between long microcracks and the total number of mapped microcracks on the horizontal thin sections. Lines on the horizontal thin sections are labelled tangential and radial (cf Figure 4-7b).*

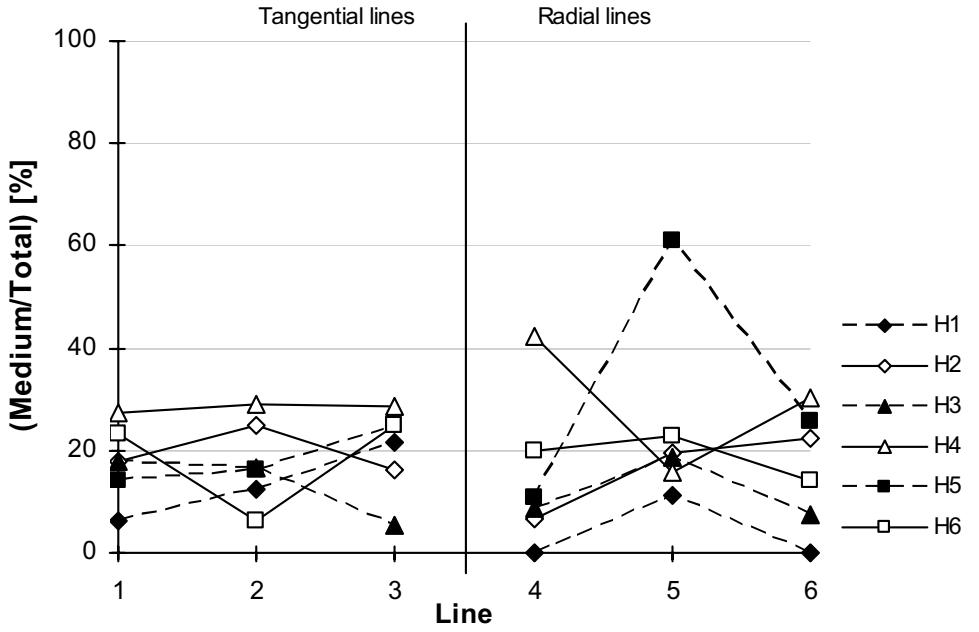

Figure B11. *Ratio between medium long microcracks and the total number of mapped microcracks on the horizontal thin sections. Lines on the horizontal thin sections are labelled tangential and radial (cf Figure 4-7b).*

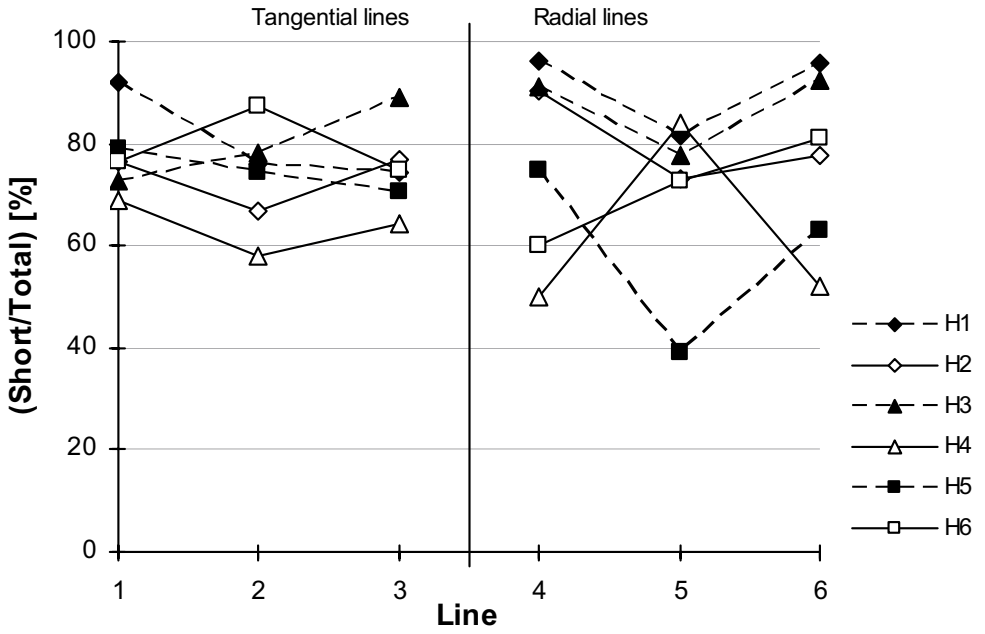

Figure B12. *Ratio between short microcracks and the total number of mapped microcracks on the horizontal thin sections. Lines on the horizontal thin sections are labelled tangential and radial (cf Figure 4-7b).*

Appendix C

Explanation of Figure 3-1

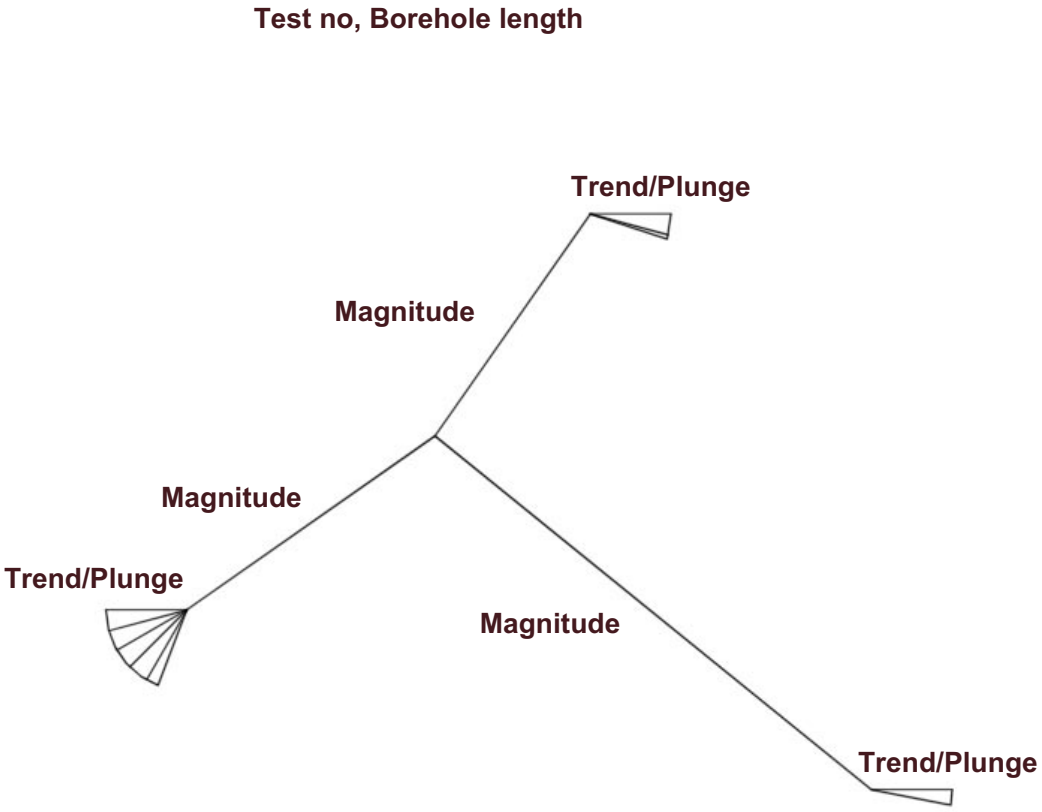

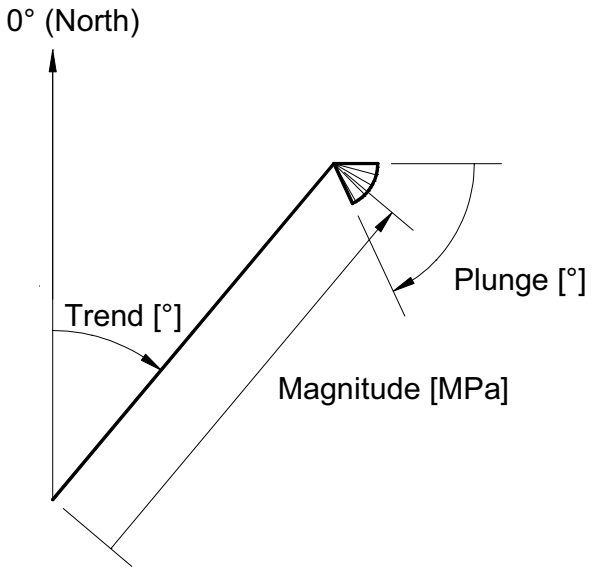

The length of each stress vector is proportional to the magnitude of the principle stress it is representing. The orientation of each stress vector corresponds to the trend of the principal stress (CW from North, which is up in the figure), and the fan-shaped symbol describes the dip of the principal stress (each fan-slice corresponds to 15°).